LIGO-P060039-00-Z

The Search for Gravitational Waves from Spinning Neutron Stars

Reinhard Prix[1] for the LIGO Scientific Collaboration

Max-Planck-Institut für Gravitationsphysik, Albert-Einstein-Institut,
Am Mühlenberg 1, 14476 Golm, Germany
Reinhard.Prix@aei.mpg.de

Summary. This paper gives an introductory overview of the search for continuous gravitational waves from spinning neutron stars. We review the current theoretical understanding of possible emission mechanisms and the expected strength of signals received on Earth. Given the substantial uncertainties involved in neutron star physics, these searches — if sufficiently sensitive — can provide important new information and constraints about neutron star physics even in the absence of detection. We describe the challenging problem of trying to detect such extremely weak signals and introduce some of the basic data analysis concepts and methods used. We conclude by summarizing the current status of the sensitivities and upper limits achieved so far. These results suggest that the search for spinning neutron stars using LIGO-I is about to enter a regime of "astrophysical relevance". Developments in the near future will make a detection of this type of source increasingly plausible.

1 Introduction

Gravitational waves (GWs), i.e. small deformations of spacetime traveling at the speed of light, are a fundamental consequence of Einstein's General Theory of Relativity. There has been no direct observation of GWs so far, although first indirect evidence was found in the observed inspiral of the binary pulsar PSR 1913+16, which agrees perfectly with the predictions of general relativity (Weisberg and Taylor (1984); Taylor and Weisberg (1989)). GWs are purely transverse, characterized by two polarization states (referred to as '+' and '×' polarizations). The two polarizations differ by a rotation of 45 degrees around the propagation axis, corresponding to the quadrupolar (spin-2) nature of the gravitational field. In contrast, the two polarization states of electromagnetic waves (which are also purely transverse), differ by a rotation of 90 degrees, reflecting the dipolar (spin-1) nature of the electromagnetic field.

Any likely sources of detectable GWs will be at astrophysical distances, thus the signals reaching Earth have very small amplitudes and are nearly plane waves. A linearized version of general relativity (e.g. see Misner et al.

(1973)) can therefore be used to describe GWs in terms of a small metric perturbation $h_{\mu\nu}$, i.e. one can write the metric as $g_{\mu\nu} = \eta_{\mu\nu} + h_{\mu\nu}$, where $|h_{\mu\nu}| \ll 1$ is the gravitational wave and $\eta_{\mu\nu}$ is the Minkowski metric of the unperturbed flat spacetime. In the so-called transverse-traceless (TT) gauge (i.e. choice of coordinates), a GW propagating along the z-direction can be written as

$$h^{\mathrm{TT}}_{\mu\nu}(t,z) = \begin{pmatrix} 0 & 0 & 0 & 0 \\ 0 & h_+ & h_\times & 0 \\ 0 & h_\times & -h_+ & 0 \\ 0 & 0 & 0 & 0 \end{pmatrix} , \tag{1}$$

with the coordinate ordering $\{t, x, y, z\}$. The effect of such a GW on two freely falling test-masses is a time-dependent change δl in their spatial distance l, which can be monitored using laser interferometry. This is the principle behind interferometric GW detectors such as the currently operating LIGO-I, GEO600, Virgo and TAMA300, or future detectors such as Advanced LIGO or the space-based LISA. The measured strain $h(t)$ of such a detector is defined as the relative length-change between the two interferometer arms l_1 and l_2 (usually at right angles to each other), namely $h(t) \equiv \delta l_1/l_1 - \delta l_2/l_2$. In the long-wavelength approximation, where the reduced wavelength of the GW is much longer than the armlength of the detector, i.e. $\lambda/2\pi \gg l_{1,2}$, it can be shown (Schutz and Tinto (1987); Thorne (1987); Jaranowski and Krolak (1994)) that the measured scalar strain $h(t)$ is related to the GW field $h^{\mathrm{TT}}_{\mu\nu}$ by

$$\begin{aligned} h(t) &= \frac{1}{2}\left(e_1^\mu e_1^\nu - e_2^\mu e_2^\nu\right) h^{\mathrm{TT}}_{\mu\nu} \\ &= F_+(t)\, h_+(t) + F_\times(t)\, h_\times(t)\,, \end{aligned} \tag{2}$$

where e_1, e_2 are unit-vectors along the two interferometer arms. The antenna-pattern (or beam-pattern) functions $F_{+,\times}(t;\psi,\boldsymbol{n}) \in [-1,1]$ describe the sensitivity of the detector to the '+' and '×' polarization, respectively, which depend on the direction $\boldsymbol{n}$ to the source (where $\boldsymbol{n}^2 = 1$), the polarization angle ψ of the wave, and the orientation of the detector. For ground-based detectors, $F_{+,\times}$ are periodic functions over one sidereal day, due to the rotation of the Earth (while for LISA the period would be one year). Explicit expressions for the antenna-pattern functions are given in Bonazzola and Gourgoulhon (1996) and Jaranowski et al. (1998). GW detectors therefore differ in several respects from classical "telescopes" for electromagnetic radiation: they are practically omni-directional (due to the wide quadrupolar antenna-pattern (2)), and they measure a single scalar function of time, $h(t)$. In this sense, they are better compared to acoustic microphones than telescopes.

The emission of GWs is generally well-described by the so-called quadrupole formula, namely

$$h^{\mathrm{TT}}_{jk} = \frac{2G}{c^4}\frac{1}{d}\left[\ddot{\mathcal{J}}_{jk}(t - r/c)\right]^{\mathrm{TT}} , \tag{3}$$

where G is Newton's gravitational constant, c is the speed of light, and d is the distance to the source. Dots denote time derivatives and $\mathcal{J}_{jk}$ is the mass-quadrupole moment of the source. The transverse-traceless operator 'TT' indicates the projection orthogonal to the direction of propagation and the removal of the trace. This expression was first derived by Einstein in 1916, using the assumption of weak internal gravity of the source, but it was later shown to be sufficient that the source is small compared to the reduced wavelength $\lambda/2\pi$ of the emitted waves (Thorne (1987); Thorne (1980)). The mass-quadrupole moment $\mathcal{J}_{jk}$ of the source is defined as the coefficient of the $1/r^3$ term in an expansion in powers of $1/r$ of the Newtonian gravitational potential (far from the source). For sources with weak internal gravity, this can directly be expressed as

$$\mathcal{J}_{jk} = \int \rho(\boldsymbol{x}) \left[x_j \, x_k - \frac{1}{3} r^2 \, \delta_{jk} \right] d^3x \,, \tag{4}$$

where $\rho(\boldsymbol{x})$ is the mass density. This is simply the Newtonian moment of inertia with the trace removed. The energy emission rate L_{GW} in GWs can be expressed in the quadrupole formalism as

$$L_{\mathrm{GW}} = \frac{1}{5} \frac{G}{c^5} \left\langle \dddot{\mathcal{J}}_{jk} \, \dddot{\mathcal{J}}^{jk} \right\rangle \,, \tag{5}$$

where $\langle ... \rangle$ denotes the time average over several periods. The quadrupole formalism shows that time-varying mass-distributions generally emit GWs. Let us now specialize to the case of a star with mass M and radius R, rotating at a frequency ν. We see from (3) that a perfectly axisymmetric star rotating around its symmetry axis will *not* emit GWs, as its quadrupole moment (4) is constant in time. Let us characterize the deviation from axisymmetry by a dimensionless number ϵ, i.e. let ϵI be the non-axisymmetric part of the moment of inertia I. Then the order of magnitude of the GW luminosity (5) can be estimated as

$$L_{\mathrm{GW}} \sim \frac{G}{c^5} \, \epsilon^2 \, I_{zz}^2 \, \nu^6 \,, \tag{6}$$

where $I_{zz} \sim M R^2$ is the moment of inertia along the rotation axis. Numerically $G/c^5 \sim 3 \times 10^{-53}$ s/J, which shows that terrestrial experiments could only produce infinitesimal amounts of GW radiation. However, rewriting this expression (e.g. see Bonazzola and Gourgoulhon (1997)) in terms of the Schwarzschild radius $R_s = 2GM/c^2$ and the rotation velocity at the surface, $V = 2\pi R \nu$, we find

$$L_{\mathrm{GW}} \sim \frac{c^5}{G} \, \epsilon^2 \left(\frac{R_s}{R} \right)^2 \left(\frac{V}{c} \right)^6 \,. \tag{7}$$

This shows that *compact objects* (i.e. with $R_s \sim R$) in rapid rotation (i.e. $V \sim c$), such as spinning neutron stars, can emit enormous GW luminosities even for small ϵ, as $c^5/G \sim 10^{52}$ W. However, spacetime is a very "stiff" medium, i.e. large amounts of energy are carried by GWs of small amplitude. This can

be seen from a similar estimate of the corresponding strain amplitude (3), namely

$$h \sim 10^2 \frac{G}{c^4} \frac{\epsilon I_{zz} \nu^2}{d} \sim 3 \times 10^{-25} \left(\frac{\epsilon}{10^{-6}}\right) \left(\frac{I_{zz}}{10^{38}\,\mathrm{kg\,m^2}}\right) \left(\frac{\nu}{100\ \mathrm{Hz}}\right)^2 \left(\frac{100\ \mathrm{pc}}{d}\right), \tag{8}$$

where the fiducial values correspond to a neutron star with typical moment of inertia, a relatively strong deviation from axisymmetry (cf. next section), at a distance of the order of the closest known neutron star, and spinning in the millisecond regime. Even for this optimistic case, the amplitude is about two orders of magnitude below the noise level of LIGO-I (cf. Fig. 3. The data-analysis challenge of detecting such GWs mainly consists of finding these extremely weak, but nearly periodic signals buried deep in the noise.

2 Continuous gravitational waves from neutron stars

In this section we give a brief overview of the current theoretical understanding of various physical mechanisms that could operate in neutron stars to produce interesting levels of GW emission (see also Owen (2006) for a recent review). As the signal-strength is generally expected to be very weak (see previous section), long integration times of the order of $T \gtrsim$ several days to years are required in order for the signal to be detectable in the noise (see next section). This GW emission therefore has to last for a long time, which characterizes the class of continuous-wave signals. The difficulties and analysis methods for these signals differ in many respects from other types of GW signals, such as bursts (e.g. from supernovae), "chirping" signals from the binary coalescence of compact objects, and the fossil stochastic background of GWs from the big bang. Note that neutron stars might also be interesting sources of burst-like GW emission, e.g. from f-mode or p-mode oscillations excited by a glitch, say, which would be damped very quickly. Another candidate for such burst-like neutron star oscillations are crustal torsional modes, which have recently been suggested by Watts and Strohmayer (2006) as a possible explanation for the high frequency oscillations observed in giant flares from Soft Gamma Repeaters. Although such GW "asteroseismology" could potentially be extremely valuable for neutron-star astrophysics (e.g. see Andersson and Kokkotas, 1998), a discussion of this type of sources is not within the scope of the present paper, as the characterization of the corresponding detection problem is very different from the continuous wave type of sources considered here.

2.1 Emission mechanisms for continuous gravitational waves

There are three classes of emission mechanisms for continuous GWs from spinning neutron stars in the LIGO frequency band: (1) non-axisymmetric

distortions of the neutron star, (2) unstable oscillation modes in the fluid part of the star (e.g. r-modes), and (3) free precession.

Non-axisymmetric distortions

Non-axisymmetric distortions cannot exist in perfect fluid stars, but in realistic neutron stars such deformations can be supported either by elastic stresses or by magnetic fields. The deformation is often expressed in terms of the *equatorial* ellipticity:

$$\epsilon \equiv \frac{I_{\mathrm{xx}} - I_{\mathrm{yy}}}{I_{\mathrm{zz}}}, \tag{9}$$

where I_{jj} are the three principal moments of inertia. This ellipticity is not to be confused with the centrifugal bulge, which is axisymmetric. A non-axisymmetric neutron star at distance a d, rotating with frequency ν around the I_{zz} axis emits monochromatic GWs of frequency $f = 2\nu$ with an amplitude

$$h_0 = \frac{16\pi^2 G}{c^4}\frac{I_{\mathrm{zz}}\nu^2}{d}\epsilon\,, \tag{10}$$

e.g. see Jaranowski et al. (1998), compare also (8). The definition of the strain-amplitude h_0 refers to a GW from an optimally oriented source with respect to the detector, as will become clearer in Sec. 3.1.

Unfortunately both the maximal possible as well as the most likely values for the non-axisymmetric deformation of neutron stars are highly uncertain. Various estimates of the maximum ellipticity ϵ sustainable by neutron stars have been given in the literature: the maximal deformation supported by the rigidity of the crust has been estimated by Ushomirsky et al. (2000) as

$$\epsilon_{\mathrm{max}} \approx 5 \times 10^{-7} \left(\frac{\sigma}{10^{-2}}\right)\,, \tag{11}$$

where σ is the breaking strain of the solid crust. The numerical coefficient in this equation is small mainly because the shear modulus of the inner crust is small compared to the pressure. The fiducial breaking strain of 10^{-2} in Eq. (11) corresponds approximately to the best terrestrial alloys. However, σ could be as high as 10^{-1} for a perfect crystal with no defects (Kittel, 2005), or several orders of magnitude smaller for an amorphous solid or a crystal with many defects. Some exotic alternatives to standard neutron star models contain solid cores, which could support considerably larger ellipticities (Owen, 2005). The most speculative and highest ellipticity models can reach up to $\epsilon_{\mathrm{max}} \approx 4 \times 10^{-4}\,(\sigma/10^{-2})$, namely for solid strange-quark stars, mostly due to their higher shear modulus.

Regardless of the maximum ellipticity supportable by shear stresses, there is a separate question of what deformations *actually* exist in neutron stars. There are several mechanisms by which the spindown of a neutron star could cause stresses in the crust to build up to the point of breaking (see Ruderman,

1969, 1976; Carter et al., 2000), usually considered in the context of glitch models. It is unclear, however, how long it would take to smooth out the mass-distribution after such a crust quake, which could possibly leave long-lived distortions of the crust.

Another possibility are accreting neutron stars in binary systems, which have a natural way of reaching and maintaining large crust deformations: the accretion flow, guided by the neutron star's magnetic field, naturally produces "hot spots" on the surface, which can lead to "hills" in hotter areas, extending down to the dense inner crust, and the ellipticity might thereby build up even to the maximum elastic value (Bildsten, 1998). The accreted material could also be held up in mountains by the magnetic field itself: the matter is a good conductor, and thus it crosses field lines relatively slowly and can pile up in mountains larger than those supportable by elasticity alone (Melatos and Payne, 2005; Payne and Melatos, 2006). Depending on the field configuration, accretion rate, and temperature, the ellipticity from this mechanism could be up to a few times 10^{-6} even for ordinary neutron stars (cf. Owen, 2006, for some discussion).

Strong internal magnetic fields could even directly produce non-axisymmetric deformation of neutron stars due to magnetic tension. A strong dipolar field that is not aligned with the rotation axis could lead to deformations of up to $\epsilon \lesssim 10^{-6}$ in the case of type-I superconducting cores (Bonazzola and Gourgoulhon, 1996). These non-aligned deformations would generally result in GW emission at *both* the first and the second harmonic of the rotation rate, i.e. $f = \nu$ and $f = 2\nu$, similar to free precession. Another possibility, suggested by Cutler (2002), is that differential rotation immediately after the birth of a neutron star could lead to large toroidal magnetic fields. Dissipation then tends to drive the symmetry axis of a toroidal field toward the star's equator, resulting in ellipticities of the order $\epsilon \sim 10^{-6}$ for toroidal magnetic fields of about $B_t \sim 10^{15}$ G.

Non-axisymmetric instabilities

At birth or during accretion, rapidly rotating neutron stars can be subject to various non-axisymmetric instabilities, which would lead to GW emission, see Andersson (2003); Stergioulas (2003) for recent reviews. If a new-born neutron star has a sufficiently high rotation rate, i.e. if the ratio $T/|W|$ of the rotational kinetic energy T to the gravitational binding energy W exceeds a critical value (typically $T/|W| \gtrsim 0.24$), it will be subject to a dynamical instability driven by hydrodynamics and gravity. Differential rotation might substantially lower the critical value to $T/|W| \gtrsim 0.14$, see Centrella et al. (2001). Through the $l = 2$ mode, this bar-mode instability will deform the star into a bar shape, which would be a strong (but likely to be short-lived, see Baiotti et al. (2006)) emitter of GWs. At lower rotation rates, the star can become unstable to secular non-axisymmetric instabilities, driven either by gravitational radiation or viscosity (e.g. Shapiro and Zane, 1998). See also

Saijo and Gourgoulhon (2006) for a recent relativistic study of the viscosity-driven instability. It is not clear, however, how effective and long-lived any these mechanisms would be in producing detectable GWs.

Gravitational radiation drives a non-axisymmetric oscillation unstable if the mode is counter-rotating with respect to the rotating frame of the star, but co-rotating with the star in the frame of a distant inertial observer. This happens when the counter-rotation rate of the mode is lower than the rotation rate of the star, and the corresponding secular instability is known as the Chandrasekhar-Friedman-Schutz (CFS) instability (Chandrasekhar, 1970; Friedman and Schutz, 1978). For polar modes such as f- or p-modes, this instability would only set in at very high rotation rates close to the breakup-limit. Therefore the most promising candidate for observable GW emission from the CFS instability is the family of r-modes, which are toroidal fluid oscillations dominated by the Coriolis force. Contrary to the polar modes, these oscillations were found to be generically unstable to the CFS instability at any finite rotation rate (Andersson, 1998; Friedman and Morsink, 1998).

Under astrophysically more realistic conditions, however, their effective instability depends on a number of highly uncertain damping mechanisms and timescales (see Stergioulas (2003) for a review). The r-mode instability has been proposed as a source of GWs (with frequency $f = 4\nu/3$) from newborn neutron stars (Owen et al., 1998) and from rapidly accreting neutron stars (Bildsten, 1998; Andersson et al., 1999). The CFS instability of the r-modes in newborn neutron stars might not be a good candidate for detection because the emission is most likely short-lived and of low amplitude. Accreting neutron stars (or quark stars) could be a better prospect for detection because the emission may be long-lived with a duty cycle near unity (Wagoner, 2002; Andersson et al., 2002).

Free precession

The third major class of emission mechanisms for continuous GWs from spinning neutron stars is free precession, i.e. the wobble of a neutron star which has a misaligned rotation axis with respect to its symmetry axis (defining the wobble angle θ_{w}). A large-angle wobble would typically produce (see Zimmermann and Szedenits, 1979; Jones and Andersson, 2002; Van Den Broeck, 2005) GWs of amplitude

$$h_0 \sim 10^{-27} \left(\frac{\theta_{\mathrm{w}}}{0.1}\right) \left(\frac{1\ \mathrm{kpc}}{d}\right) \left(\frac{\nu}{500\ \mathrm{Hz}}\right)^2 , \tag{12}$$

where θ_{w} is measured in radians. Generally, free precession results in emission at (approximately) the rotation rate ν and twice the rotation rate, i.e. $f = \nu + \nu_{\mathrm{prec}}$ (where ν_{prec} is the precession frequency) and $f = 2\nu$. Free precession may be longer lived than previously thought (Cutler and Jones, 2001), but the amplitude is still quite small, which might make this mechanism relevant only for second-generation interferometers such as Advanced LIGO.

2.2 Loudest expected signal from isolated neutron stars

Current models of stellar evolution suggest that our Galaxy contains of order 10^9 neutron stars, while only of order 10^5 are expected to be active pulsars. Up to now only about 1700 pulsars have been observed (see Manchester et al., 2005); there are numerous reasons for this, including selection effects and the fact that many have faint emission. Although there is great uncertainty in the physics of the GW emission mechanisms and the strength of individual sources, one can argue for a statistical upper limit on the expected strongest GW signals from the galactic population of neutron stars, which is almost independent of individual source physics. The argument goes back to Blandford, and an updated version (due to Cutler) is found in Abbott et al. (2006b), of which we only summarize the main assumptions and the result. One can make the (optimistic) assumption that there exists a class of neutron stars that are born rapidly rotating, spinning down due to GWs, and that they are distributed uniformly throughout the galactic disc. Further assuming a constant overall galactic birthrate, one can convert these assumptions into a distribution of neutron stars with respect to GW strain and frequency, and find that there is a 50% chance that the strongest signal within the LIGO band has an amplitude of at least

$$h_0 \sim 4 \times 10^{-24} \,. \tag{13}$$

Note, however, that this is a purely statistical argument, and it is possible that the closest strong emitter is either far closer or further away than the typical distance expected from a random distribution of supernovae. This is an upper limit in the sense that the assumptions are optimistic, and one would expect a lower amplitude if some of them were not true.

2.3 The spindown limit for known pulsars

While the statistical argument of the previous section applies to the general population of unknown neutron stars in the galaxy, an even more robust upper limit on the maximum amplitude h_0 can be derived for pulsars with known spindown $\dot{\nu}$ and distance d. For simplicity, let us consider the case of spinning neutron stars with a non-axisymmetric deformation ϵ, emitting GWs at frequency $f = 2\nu$. In this case the GW luminosity (5) can be written explicitly as

$$L_{\mathrm{GW}} = \frac{1}{10}\frac{G}{c^5}(\pi\nu)^6 \, I_{zz}^2 \, \epsilon^2 \,. \tag{14}$$

If we assume that the GW emission is powered *only* by the rotational energy of the spinning neutron star, namely $E_{\mathrm{rot}} = 2\,\pi^2\nu^2 I_{zz}$, then we have the inequality

$$L_{\mathrm{GW}} \leq -\dot{E}_{\mathrm{rot}} = -2\pi^2 \left(2 I_{zz}\, \nu\dot{\nu} + \nu^2 \, \dot{I}_{zz}\right) \,. \tag{15}$$

For constant moment of inertial, $\dot{I}_{zz} = 0$, this yields an upper limit on the quadrupolar deformation $\epsilon \leq \epsilon_{\rm sd}$, namely

$$\epsilon_{\rm sd} = \sqrt{\frac{5c^5}{2(4\pi)^4 G\, I_{zz}} \frac{|\dot{\nu}|}{\nu^5}}\,. \tag{16}$$

Substituting this into Eq. (10), one obtains the following upper limit $h_0 \leq h_{\rm sd}$ on the GW amplitude:

$$h_{\rm sd} = \frac{1}{d}\sqrt{\frac{5G\, I_{zz}}{2c^3} \frac{|\dot{\nu}|}{\nu}}\,. \tag{17}$$

2.4 Maximum expected signal from accreting neutron stars

The statistical upper limit (13) on h_0 is not applicable to accreting neutron stars, since energy conservation plays a crucial role in the argument. However, if accretion replenishes the star's angular momentum, a different argument can be made, independent of the details of the emission mechanism. In this case $h_0^{\rm max}$ is set by the X-ray luminosity of the brightest X-ray source. The basic idea is that if the angular momentum lost in GWs is replenished by accretion, then the strongest GW emitters are those accreting at the highest rate, such as low-mass X-ray binaries (LMXBs). The accreted gas hitting the surface of the neutron star is heated to 10^8 K and emits X-rays. As noted several times (Papaloizou and Pringle, 1978; Wagoner, 1984; Bildsten, 1998), if one assumes the spindown torque from GW emission to be in equilibrium with the accretion torque, then h_0 is directly related to the X-ray luminosity, namely

$$h_0 \approx 5 \times 10^{-27} \left(\frac{300\ {\rm Hz}}{\nu}\right)^{1/2} \left(\frac{F_{\rm x}}{10^{-8}\ {\rm erg\,cm^{-2}\,s^{-1}}}\right)^{1/2}, \tag{18}$$

where $F_{\rm x}$ is the observed X-ray flux. It is interesting to note that this expression does not explicitly depend on the distance of the system, which is implicitly contained by using of the observed X-ray flux on Earth (both the GW and X-ray flux decrease with $1/d^2$). This theoretical argument is supported by the observation that the frequencies of most LMXBs seem to cluster in a fairly narrow range of 270 Hz $\lesssim \nu \lesssim$ 620 Hz (see Chakrabarty et al., 2003). Since most neutron stars will have accreted enough matter to spin them up to near their theoretical maximum spin frequencies, estimated at $\nu_{\rm max} \sim 1400$ Hz (e.g. see Cook et al. (1994)), the observed spin distribution is hard to explain without a competing mechanism to counter the spin-up. Since the GW torque scales as $\propto \nu^5$, gravitational radiation is also a natural explanation for the rather narrow clustering of observed frequencies. If this argument holds, then the accreting neutron star that is brightest in X-rays (namely Sco X-1) should also be the strongest source of GWs. Using the known X-ray flux of Sco X-1, its expected GW emission would have an amplitude of

$$h_0 \approx 3 \times 10^{-26} \left(\frac{540 \text{ Hz}}{f} \right)^{1/2} , \tag{19}$$

where the frequency f is not well known, but assumed to be in the range of several hundred Hz. This signal could in principle be detectable by second-generation interferometers such as Advanced LIGO (see Fig. 4).

3 Data analysis of continuous gravitational waves

As discussed in the previous section, continuous GWs reaching Earth are expected to be exceedingly weak, even compared to the sensitivities of the current generation of detectors. In order to be able to dig such signals out of the noise, one typically has to "integrate" for several days up to months by "matching" the data with a target signal ("template") of given parameters. This is the basic concept of *matched filtering*, which is the optimal method in a statistical sense (made more precise later). See also Jaranowski and Królak (2005) for a recent review of the detection problem of continuous GWs.

As noted in the introduction, GW detectors are practically omni-directional. Due to the long integration time, however, continuous GWs become extremely well-localized, not only in frequency but also in sky-position. A mismatch in frequency between the true signal and a template results in a phase mismatch that is growing with observation time, and thereby rapidly degrading the output of the (mis-)matched filter. Similarly, the Doppler effect from the daily rotation and orbital motion of the Earth modulates signals in a way that depends sensitively on the direction from which they are coming. The templates therefore need to be sky-position specific, and the required precision increases again with observation time.

In the case of *wide-parameter searches* for unknown sources, this makes it very expensive in computing cost to increase the observation time, as it requires a much finer search in the parameter space of possible signals. There is also a purely statistical effect limiting the sensitivity of such searches: the more trials (i.e. targeting of different points in parameter space) one performs, the more candidates are expected from noise fluctuations alone to cross a given threshold. Therefore, a higher detection threshold is required, which reduces the sensitivity.

On the other hand, fully *targeted searches* for GW sources with known parameters (such as pulsars with known sky-position and frequency evolution) are not affected by these difficulties and can attain the best possible sensitivity by coherently integrating all the available data.

3.1 The general form of the signal

A general, elliptically polarized GW can be written in the reference frame of the source as

$$h_+(\tau) = A_+ \cos\Phi(\tau)\,, \quad h_\times(\tau) = A_\times \sin\Phi(\tau)\,, \tag{20}$$

where $h_{+,\times}$ are the two polarization states of $h^{\mathrm{TT}}_{\mu\nu}$ as given in (1), using coordinates aligned with the principal polarization axes of the coherent GW. Assuming a quasi-monochromatic signal with slowly-varying intrinsic frequency $f(\tau)$, the signal phase $\Phi(\tau)$ can be Taylor-expanded as

$$\Phi(\tau) = \phi_0 + \phi(\tau)\,, \quad \phi(\tau) = 2\pi \sum_{k=0}^{s} \frac{f^{(k)}(\tau_{\mathrm{ref}})}{(k+1)!}\, \Delta\tau^{k+1}\,, \tag{21}$$

where $\Delta\tau \equiv \tau - \tau_{\mathrm{ref}}$, and τ_{ref} is the reference time, at which the initial phase ϕ_0 and the $s+1$ spin parameters $f^{(k)} \equiv d^k f(\tau)/d\tau^k$ are defined.

Let $\boldsymbol{n} = (\cos\delta\,\cos\alpha, \cos\delta\,\sin\alpha, \sin\delta)$ be the unit vector pointing to the source, expressed in equatorial coordinates using the standard celestial angles α (right ascension) and δ (declination). The wave-frame is then completely determined by $\boldsymbol{n}$ and the "polarization angle" ψ, which describes the orientation of the polarization axes with respect to the equatorial-coordinate system. Following the conventions of Bonazzola and Gourgoulhon (1996), ψ can be defined as the angle between the direction $\boldsymbol{n} \times \boldsymbol{Z}$ and the $\boldsymbol{x}$-axis of the TT wave-frame (corresponding to the '+' polarization), where $\boldsymbol{Z} = (0, 0, 1)$ is the unit-vector pointing to the celestial north pole. As shown in Jaranowski et al. (1998), the dependency of the antenna-pattern functions $F_{+,\times}$ on the wave-frame orientation $\{\boldsymbol{n}, \psi\}$ can be separated as

$$F_+(t; \boldsymbol{n}, \psi) = a(t; \boldsymbol{n})\, \cos 2\psi + b(t; \boldsymbol{n})\, \sin 2\psi\,, \tag{22}$$

$$F_\times(t; \boldsymbol{n}, \psi) = b(t; \boldsymbol{n})\, \cos 2\psi - a(t; \boldsymbol{n})\, \sin 2\psi\,, \tag{23}$$

where the expressions for the (detector-dependent) functions $a(t; \boldsymbol{n})$, $b(t; \boldsymbol{n})$ are given in Eqs. [12,13] of Jaranowski et al. (1998).

In the detector frame the signal amplitude is modulated by the rotating antenna pattern $F_{+,\times}(t)$, as seen in Eq. (2). More importantly, the signal is also Doppler-modulated by the relative motion of the detector with respect to the source. This can be expressed as a relation between the detector arrival time t of a wave-front that left the source at time $\tau(t)$. Let us consider the most general case of a neutron star in a binary system with orbital parameters $\mathbf{b}$ at a sky-position $\boldsymbol{n}$. The timing relation $\tau(t)$ can then be written as

$$\tau(t; \boldsymbol{n}, \mathbf{b}) = t + \Delta_\odot(t; \boldsymbol{n}) - d(t)/c + \Delta_\circledast(t; \mathbf{b})\,, \tag{24}$$

where $\Delta_\odot$ is the time-delay between the wave-front arrival time at the solar-system barycenter (SSB) and the detector, $\Delta_\circledast$ is the delay between the neutron star and the binary-system barycenter (BSB), and $d(t)$ is the distance between the BSB and the SSB. Note that $d(t)$ is usually assumed to be constant and is neglected. This entails no loss of generality as its effects can be absorbed into an apparent frequency-evolution of the source. Note that obviously $\Delta_\circledast = 0$ for isolated neutron stars. The delay $\Delta_\odot$ between the SSB and the detector can be written more explicitly as

$$\Delta_{\odot}(t;\boldsymbol{n}) = \frac{\boldsymbol{r}(t)\cdot\boldsymbol{n}}{c} + \Delta_{E\odot}(t;\boldsymbol{n}) + \Delta_{S\odot}(t;\boldsymbol{n})\,, \tag{25}$$

where $\boldsymbol{r}(t)$ is the vector from the SSB to the detector location. The first term is known as the Roemer-delay, while $\Delta_{S\odot}$ is the general-relativistic Shapiro delay caused by the gravitational field of the sun, and $\Delta_{E\odot}$ is the so-called Einstein delay, caused by the gravitational redshift and time dilation at Earth (see Taylor and Weisberg (1989) for details). The effects of both Shapiro and Einstein delay are generally much smaller than the Newtonian Roemer-delay $\boldsymbol{r}\cdot\boldsymbol{n}/c$. The time delays $\Delta_{\circledast}$ within the binary system of the source have exactly the same form as (25). Inserting the timing relation (24) into the phase (21) in the source frame, we see that the phase evolution in the detector frame has the general form

$$\phi(\tau) = \phi(t;\boldsymbol{\lambda})\,, \quad \text{where} \quad \boldsymbol{\lambda} \equiv \{f^{(k)},\, \boldsymbol{n},\, \mathbf{b}\}\,, \tag{26}$$

which defines the "Doppler parameters" $\boldsymbol{\lambda}$. Putting all the pieces together, we can now express the measured strain signal $h(t)$ as

$$\begin{aligned} h(t;\mathcal{A},\boldsymbol{\lambda}) = {} & F_+(t;\boldsymbol{n},\psi)\, A_+ \cos\left[\phi_0 + \phi(t;\boldsymbol{\lambda})\right] \\ & + F_\times(t;\boldsymbol{n},\psi)\, A_\times \sin\left[\phi_0 + \phi(t;\boldsymbol{\lambda})\right]\,, \end{aligned} \tag{27}$$

where we defined the set of four "amplitude parameters" $\mathcal{A} \equiv \{A_+, A_\times, \psi, \phi_0\}$. Using the general form (22) of the antenna-pattern functions $F_{+,\times}$, it is now easy to see that the dependencies on the amplitude and Doppler parameters can be explicitly separated, namely

$$h(t;\mathcal{A},\boldsymbol{\lambda}) = \sum_{\mu=1}^{4} \mathcal{A}^\mu\, h_\mu(t;\boldsymbol{\lambda})\,, \tag{28}$$

in terms of four basis waveforms

$$h_1(t;\boldsymbol{\lambda}) = a(t;\boldsymbol{n})\,\cos\phi(t;\boldsymbol{\lambda})\,, \quad h_2(t;\boldsymbol{\lambda}) = b(t;\boldsymbol{n})\,\cos\phi(t;\boldsymbol{\lambda})\,, \tag{29}$$

$$h_3(t;\boldsymbol{\lambda}) = a(t;\boldsymbol{n})\,\sin\phi(t;\boldsymbol{\lambda})\,, \quad h_4(t;\boldsymbol{\lambda}) = b(t;\boldsymbol{n})\,\sin\phi(t;\boldsymbol{\lambda})\,, \tag{30}$$

and the amplitude vector $\mathcal{A}^\mu$, defined as

$$\begin{aligned} \mathcal{A}^1 &= \;\; A_+\cos\phi_0\,\cos 2\psi - A_\times\,\sin\phi_0\,\sin 2\psi\,, \\ \mathcal{A}^2 &= \;\; A_+\cos\phi_0\,\sin 2\psi + A_\times\,\sin\phi_0\,\cos 2\psi\,, \\ \mathcal{A}^3 &= -A_+\sin\phi_0\,\cos 2\psi - A_\times\,\cos\phi_0\,\sin 2\psi\,, \\ \mathcal{A}^4 &= -A_+\sin\phi_0\,\sin 2\psi + A_\times\,\cos\phi_0\,\cos 2\psi\,. \end{aligned} \tag{31}$$

Note that there is some residual gauge-freedom in the amplitude parameters $\mathcal{A}$, as the signal (27) is seen to be invariant under any of the following transformations:

$$(1)\;\; \psi \to \psi + \pi/2, \quad \phi_0 \to \phi_0 + \pi\,, \tag{32}$$

$$(2)\;\; \phi_0 \to \phi_0 + \pi, \quad A_{+,\times} \to -A_{+,\times}\,, \tag{33}$$

$$(3)\;\; \psi \to \psi + \pi/4, \quad \phi_0 \to \phi_0 - \pi/2, \quad A_+ \leftrightarrow A_\times\,. \tag{34}$$

Note that different emission mechanisms of continuous GWs result in different expressions for the amplitude parameters $\mathcal{A}$ in terms of the source parameters, and in different relations between the rotation frequency ν of the neutron star and the GW frequency f in (21). Some interesting special cases are triaxial neutron stars rotating around a principal axis, in which case $f = 2\,\nu$, free precession, which emits additional signal at $f \approx \nu$, and r-mode oscillations emitting at $f = 4\nu/3$, as discussed in Sec. 2. However, in order to simplify the discussion, it is often convenient to express the amplitudes $A_{+,\times}$ in terms of the source parameters of a non-precessing triaxial neutron star (e.g. Jaranowski et al., 1998), namely

$$A_+ = \frac{1}{2} h_0 \left(1 + \cos^2 \iota\right) , \quad A_\times = h_0 \, \cos \iota \, , \tag{35}$$

where h_0 is the overall amplitude, given in (10), and ι is the angle between the spin-axis of the neutron star and the line-of-sight $\boldsymbol{n}$. This is conceptually the simplest source model, and it does not entail any loss of generality, as the mapping between $\{h_0, \cos\iota\}$ and $A_{+,\times}$ is one-to-one.

3.2 Signals in noise

In practice, the strain $x(t)$ measured by a detector is mainly dominated by noise $n(t)$, such that even in the presence of a signal $h(t)$ we have

$$x(t) = n(t) + h(t; \mathcal{A}, \boldsymbol{\lambda}) \, . \tag{36}$$

The noise can stem from a variety of sources, some of the dominant contributions are seismic noise and gravity-gradient noise at low frequencies, and shot noise at high frequencies (e.g. see Thorne (1987) and Abbott et al. (2004a) for more details). The measured output is not a continuous function of time, but a discrete time series of data points $x_i = x(t_i)$ with $t_i = i\,\Delta t$, sampled at a finite rate $f_{\mathrm{samp}} = 1/\Delta t$, e.g. for LIGO and GEO600 $f_{\mathrm{samp}} = 16\,384$ Hz. For convenience of notation, however, a continuous-time formulation is often used. Let us make the idealized assumption of Gaussian stationary noise n_i with zero mean and covariance $\gamma_{jk} \equiv E[n_j \, n_k]$, where $E[.]$ denotes the expectation-value. If we define the scalar product $(x||y)$ of two (real-valued) time series x_i and y_i as

$$(x||n) \equiv \sum_{j,l} n_j \, \gamma_{jl}^{-1} \, n_k \, , \tag{37}$$

then the probability of a (pure-noise) time series $\{n_j\}_{j=0}^{M-1}$ can be written as

$$P\left(\{n_j\}|\gamma\right) = (2\pi)^{-M/2} \, |\gamma|^{-1/2} \, e^{-\frac{1}{2}(n||n)} \, . \tag{38}$$

In the continuum limit of $\Delta t \to 0$, the scalar product (37) can be shown (cf. Finn, 1992) to converge to the expression

$$(x||y) \overset{\Delta t \to 0}{\to} 4\Re \int_0^\infty \frac{\widetilde{x}(f)\,\widetilde{y}^*(f)}{S_\mathrm{n}(f)}\,df\,, \tag{39}$$

which is the classical Wiener filter of matched-filtering theory (Wainstein and Zubakov, 1962). Here $\widetilde{x}(f)$ is the Fourier transform of $x(t)$, and * denotes complex conjugation. $S_\mathrm{n}(f)$ is the single-sided power spectral density, which is defined as the Fourier transform of the auto-correlation function, i.e.

$$S_\mathrm{n}(f) = 2\int_{-\infty}^{\infty} E[n(0)\,n(t)]\,e^{-i2\pi\,ft}\,dt\,. \tag{40}$$

In practice, this definition is not very useful for computing S_n, but an estimate for S_n can be obtained from the finite discrete time series $\{n_j\}$ using the Wiener-Khintchine theorem, namely

$$S_\mathrm{n}(f) \approx \frac{2}{T_\mathrm{obs}} E\left[|\widetilde{n}(f)|^2\right]\,, \tag{41}$$

which holds exactly in the limit of infinite duration T_obs of the time-series, i.e. when $T_\mathrm{obs} \equiv M\,\Delta t \to \infty$. Here $\widetilde{n}(f)$ is the discrete Fourier transform of n_j, defined as

$$\widetilde{n}(f) = \Delta t \sum_{j=0}^{M-1} n_j\,e^{-i2\pi\,f\,j\,\Delta t}\,. \tag{42}$$

The quantity $\sqrt{S_\mathrm{n}(f)}$ (which has units of $\mathrm{Hz}^{-1/2}$) is the most commonly-used measure of the noise performance GW detectors, e.g. see Fig. 3. Note that in the case of nearly-monochromatic signals $h(t)$, as considered here, only a very narrow frequency band around the signal frequency f_0 will contribute to the scalar product (39). In this case, $S_\mathrm{n}(f)$ can be approximated as constant in the neighborhood of f_0, and the scalar product therefore simplifies to

$$(x||y) \approx \frac{2}{S_\mathrm{n}(f_0)} \int_0^{T_\mathrm{obs}} x(t)\,y(t)\,dt\,. \tag{43}$$

Using (36) and (38), the probability of measuring a strain $x(t)$ in the presence of Gaussian noise $n(t)$ and a signal $h(t;\mathcal{A},\boldsymbol{\lambda})$ can be expressed as

$$P(x|\mathcal{A},\boldsymbol{\lambda},S_\mathrm{n}) \propto e^{-\frac{1}{2}(x-h||x-h)}\,. \tag{44}$$

The signal-to-noise ratio (SNR) of matched filtering is conventionally defined as $\rho \equiv \sqrt{(h||h)}$, and for continuous GWs it is straightforward to show (e.g. Jaranowski et al., 1998; Cutler and Schutz, 2005; Prix, 2006) that the SNR scales as

$$\rho = \sqrt{(h||h)} \propto \frac{h_0}{\sqrt{S_\mathrm{n}}}\,\sqrt{T_\mathrm{obs}\,\mathcal{N}}\,, \tag{45}$$

with the observation time T_obs and the number of equal-sensitivity detectors $\mathcal{N}$. This illustrates why it is essential for continuous-wave searches to integrate

the data for the longest possible observation time T_{obs} (and use as many sensitive detectors $\mathcal{N}$ as possible). There are two different ways of proceeding from this point, depending on the paradigm of statistics used: Bayesian or frequentist. These approaches yield sometimes similar-looking answers (especially in Gaussian noise), but they are based on fundamentally different interpretations and provide different tools in practice. The conceptual difference between the two frameworks lies in the meaning of "probability", while the axioms for *calculating* with those probabilities are the same in both cases.

3.3 Frequentist framework

The frequentist approach is based on the frequency-interpretation of probability: the probability $P(A)$ of an event A is defined as the limiting fraction of events A in an infinite number of "identical"[1] trials. The frequentist detection problem is formulated as one of hypothesis testing: let H_0 be the hypothesis that there is no signal in the data, i.e. $h = 0$, and H_1 that there is a nonzero signal h. One then seeks a criterion to decide in an optimal way between the two hypothesis given the measurement $x(t)$. This is achieved by computing a detection statistic $\Lambda(x)$, and setting a threshold Λ^* such that H_0 is accepted if $\Lambda(x) < \Lambda^*$, while H_1 is accepted otherwise. From the probability distribution (44) of $x(t)$, one can calculate $P(\Lambda|H_0)$ and $P(\Lambda|H_1)$ for the two hypothesis. This allows us to define the "false alarm" probability $\alpha(\Lambda^*)$, namely

$$\alpha(\Lambda^*) \equiv \int_{\Lambda^*}^{\infty} P(\Lambda|H_0)\, d\Lambda\,, \tag{46}$$

which is the probability of a threshold crossing despite H_0 being true. Similarly, we define the "false dismissal" probability $\beta(\Lambda^*|h)$ of a signal h as

$$\beta(\Lambda^*|h) \equiv \int_{-\infty}^{\Lambda^*} P(\Lambda|H_1)\, d\Lambda\,, \tag{47}$$

which is the probability that the threshold is not crossed, even though H_1 is true. The detection probability η is simply the complement, namely $\eta(\Lambda^*|h) = 1 - \beta$. A standard criterion for the optimality of a hypothesis test $\Lambda(x)$ is that the test should maximized the detection probability $\eta(h|\Lambda^*)$ at a given false-alarm rate $\alpha(\Lambda^*)$. According to the Neyman-Pearson lemma, this optimal test is the so-called likelihood ratio, which is defined as

$$\Lambda(x; h) \equiv \frac{P(x|h)}{P(x|0)}\,. \tag{48}$$

Applying this to our Gaussian detection problem (44), one finds

[1] Obviously, the trials cannot truly be identical or they would always yield the same result.

$$\ln \Lambda(x;h) = (x||h) - \frac{1}{2}(h||h)\,, \tag{49}$$

which is the well-known expression for the matched-filtering amplitude. If some of the parameters of the signal $h(t;\mathcal{A},\boldsymbol{\lambda})$ are unknown, one has to find the *maximum* of $\ln\Lambda$ as a function of the unknown parameters.

The $\mathcal{F}$-statistic

In targeted searches of GWs from known pulsars, the Doppler parameters $\boldsymbol{\lambda}$, i.e. sky-position $\boldsymbol{n}$ and spin $f(\tau)$, are usually well known, but even in this case one has generally no information about the four amplitude parameters $\mathcal{A}$, which would have to be scanned with different templates. However, as shown in Jaranowski et al. (1998), the maximization over the amplitude parameters $\mathcal{A}$ can be performed analytically, thereby decreasing the number of unknown parameters that need to be searched over explicitly. Inserting the factored expression (28) for the filters $h(t;\mathcal{A},\boldsymbol{\lambda})$ into (49), we obtain

$$\ln \Lambda(x;\mathcal{A},\boldsymbol{\lambda}) = \mathcal{A}^\mu\, x_\mu - \frac{1}{2}\mathcal{A}^\mu\mathcal{A}^\nu\,\mathcal{M}_{\mu\nu}\,, \tag{50}$$

with implicit summation over $\mu,\nu = 1,2,3,4$, and where we defined

$$x_\mu(\boldsymbol{\lambda}) \equiv (\boldsymbol{x}||h_\mu)\,, \quad \text{and} \quad \mathcal{M}_{\mu\nu}(\boldsymbol{\lambda}) \equiv (h_\mu||h_\nu)\,. \tag{51}$$

We can now maximize $\ln\Lambda$ over $\mathcal{A}^\mu$ to obtain the maximum-likelihood (ML) estimators $\mathcal{A}^\mu_{\mathrm{ML}}$ from the data $x(t)$, namely

$$\frac{\partial \ln\Lambda}{\partial \mathcal{A}^\mu} = 0 \quad \Longrightarrow \quad \mathcal{A}^\mu_{\mathrm{ML}} = \mathcal{M}^{\mu\nu}\, x_\nu\,, \tag{52}$$

where $\mathcal{M}^{\mu\alpha}\mathcal{M}_{\alpha\nu} = \delta^\mu_\nu$. Re-inserting these ML-estimators into (50), we obtain a new, partially-maximized detection statistic, namely

$$2\mathcal{F}(x;\boldsymbol{\lambda}) = x_\mu\,\mathcal{M}^{\mu\nu}\,x_\nu\,, \tag{53}$$

which is the so-called $\mathcal{F}$-statistic.[2] Contrary to (50), the $\mathcal{F}$-statistic only depends on the Doppler parameters $\boldsymbol{\lambda}$. The coherent multi-detector generalization of the $\mathcal{F}$-statistic was recently derived by Cutler and Schutz (2005), but for simplicity we restrict the following discussion to the single-detector case. In the presence of a signal $h(t;\mathcal{A}_{\mathrm{sig}},\boldsymbol{\lambda}_{\mathrm{sig}})$, the expectation value of the $\mathcal{F}$-statistic with perfectly matched Doppler parameters, $\boldsymbol{\lambda} = \boldsymbol{\lambda}_{\mathrm{sig}}$, is given by

$$E[2\mathcal{F}] = 4 + \rho^2\,, \tag{54}$$

where ρ is the optimal SNR defined previously in (45). One can show (cf. Jaranowski et al. (1998); Cutler and Schutz (2005)) that $2\mathcal{F}$ is a random

[2] Not to be confused with the F-statistic or the F-test in the statistical literature

variable with a χ^2-distribution with 4 degrees of freedom and a non-centrality parameter ρ^2 (for the definition of the non-central χ^2-distribution, see for example Abramowitz and Stegun (1964)). In the absence of a signal, i.e. $\rho = 0$, this reduces to the central χ^2-distribution, namely

$$P(2\mathcal{F}; 0) = \frac{1}{2}\,\mathcal{F}\,e^{-\mathcal{F}}\,. \tag{55}$$

Using the known probability distribution of $2\mathcal{F}$, we can compute the false-alarm $\alpha(2\mathcal{F}^*)$ and false-dismissal probability $\beta(2\mathcal{F}^*; \rho^2)$ for a threshold $2\mathcal{F}^*$ and an SNR ρ. The false-alarm (46) is easily integrated and yields

$$\alpha(2\mathcal{F}^*) = (1 + \mathcal{F}^*)\,e^{-\mathcal{F}^*}\,, \tag{56}$$

while the false-dismissal probability (47) generally needs to be integrated numerically. If we choose a false-alarm rate of $\alpha(2\mathcal{F}^*) = 1\%$, say, this determines the detection threshold as $2\mathcal{F}^* \approx 13.3$. With this threshold, the required SNR for a false-dismissal rate of 10%, say, is given by $\beta(2\mathcal{F}^*; \rho^2) = 10\%$, which results in $\rho \approx 4.5$. Using Eq. [93] of Jaranowski et al. (1998), which relates the *average* SNR $\langle\rho\rangle$ (averaged over sky-location $\boldsymbol{n}$, orientation $\cos\iota$ and polarization ψ), to the amplitude h_0, we obtain the smallest average amplitude $\langle h_0\rangle$ that would be detectable with a 1% false-alarm and 10% false-dismissal rate, namely

$$\langle h_0\rangle^{\beta=10\%}_{\alpha=1\%} \approx 11.4\,\sqrt{\frac{S_\mathrm{n}}{T_\mathrm{obs}}}\,, \tag{57}$$

where T_obs is the coherently-integrated observation time. This is a useful measure of the sensitivity of a search. Note, however, that the false-alarm rate (56) refers to a *single* trial, and therefore this sensitivity-estimate only applies to targeted, single-template searches. When using a coherent network of detectors with respective noise floors S_X, the combined noise-floor to use in (57) is given by $S_\mathrm{n}^{-1} = \sum S_\mathrm{X}^{-1}$. Therefore, the combined sensitivity of $\mathcal{N}$ equal-noise detectors is improved by a factor of $\sqrt{\mathcal{N}}$. In the case of LIGO I, the combined design-sensitivity of H1, L1 and H2 would be roughly a factor $\sqrt{2.25}$ better, as H2 has only half the armlength of H1 and L1. Advanced LIGO will instead consists of three 4 km-armlength interferometers, and the combined detector would therefore be a factor $\sqrt{3}$ more sensitive.

The standard frequentist upper limit of confidence C is defined as the amplitude h_0^C of signals that would exceed the measured value $2F_0$ in a fraction C of trials, i.e.

$$C = \int_{2\mathcal{F}_0}^{\infty} P(2\mathcal{F}|h_0^C)\,d2\mathcal{F}\,, \tag{58}$$

which will typically be determined by Monte-Carlo integration. Note that, contrary to the Bayesian approach described below, this is not a statement about the confidence that the true value of h_0 is contained in the interval $[0, h_0^C]$, but about the frequency with which the so-constructed interval would

contain the true value in repeated experiments. For a more detailed discussion and an elegant method of constructing frequentist confidence intervals, see Feldman and Cousins (1998).

3.4 Bayesian analysis

Bayesian statistics is built on a different concept of probability, quantifying the degree of certainty (or "degree of belief") of a statement being true (see Loredo (1990); Sivia (1996) for discussion and references). A more detailed discussion of the application of Bayesian statistics to the problem of detecting continuous GWs is found in Dupuis and Woan (2005) and Christensen et al. (2004).

Freed from the narrower frequentist definition, one can assign probabilities $P(A|I) \in [0,1]$ to any statement A within some model I, quantifying one's (possibly incomplete) knowledge about the truth of A. The probabilities $P(A|I) = 1$ and $P(A|I) = 0$ reflect the extreme cases of certainty about A being true or false, respectively. The axioms of probability provide a natural framework to calculate with such quantified partial knowledge. A central tool in this approach is Bayes' theorem (an elementary consequence of the axioms of probability), namely

$$P(A|x, I) = P(x|A, I)\,\frac{P(A|I)}{P(x|I)}\,. \tag{59}$$

Using this together with (44), we can express the "posterior probability" of a signal $h(t; \mathcal{A}, \boldsymbol{\lambda})$ being present *given* the measurement $x(t)$, namely

$$P(\mathcal{A}, \boldsymbol{\lambda}|x, I) = k\, P(x|\mathcal{A}, \boldsymbol{\lambda}, I)\, P(\mathcal{A}, \boldsymbol{\lambda}|I)\,, \tag{60}$$

where k is a normalization constant. The factor $P(\mathcal{A}, \boldsymbol{\lambda}|I)$ is the so-called "prior probability", which expresses the previous knowledge about the signal, either from other measurements or from theoretical considerations. Eq. (60) quantifies how the state of knowledge is transformed from the prior $P(\mathcal{A}, \boldsymbol{\lambda}|I)$ to the posterior $P(\mathcal{A}, \boldsymbol{\lambda}|x, I)$ in the light of new information $x(t)$. One of the most controversial aspects of Bayesian statistics is the assignment of prior probabilities. One often tries to use a prior reflecting complete "ignorance" or minimal bias (a common choice is a flat prior, i.e. $P(\mathcal{A}, \boldsymbol{\lambda}|I) = \text{const.}$), but this is not unproblematic and there is no unique choice of such a zero-information prior. Using the likelihood function (44) together with (60), we find the posterior

$$P(\mathcal{A}, \boldsymbol{\lambda}|x, I) = k'\, P(\mathcal{A}, \boldsymbol{\lambda}|I)\, \Lambda(x; \mathcal{A}, \boldsymbol{\lambda})\,, \tag{61}$$

where k' is another normalization constant. We see that we are naturally lead back to the likelihood ratio (49). However, the statistical interpretation is very different from the frequentist framework, as (61) explicitly determines the

probability of a signal with certain parameters being present, while one cannot assign meaningful frequentist probabilities to such statements. Equation (61) formulates the detection problem in terms of *parameter estimation* of the signal, while the frequentist approach is typically based on *hypothesis testing*.

A powerful tool of the Bayesian framework is the so-called *marginalization* over "nuisance parameters". Let us assume for simplicity that we have performed a targeted, single-template search were the Doppler parameters $\boldsymbol{\lambda}$ are known. If we want to express the posterior of a subset of the unknown amplitude parameters $\mathcal{A}$, e.g. we might be most interested in $P(h_0|x, I)$, say, then this can be computed by summing the full posterior over all the possible values of the "uninteresting" parameters $\cos\iota$, ψ and ϕ_0, i.e.

$$P(h_0|x, I) \propto \int P(\mathcal{A}|x, I)\, d\phi_0\, d\psi\, d\cos\iota\,. \tag{62}$$

The Bayesian way of determining an upper limit $h_0^{\mathbf{C}}$ of confidence $\mathbf{C}$ is simply by solving the equation

$$\mathbf{C} = \int_0^{h_0^{\mathbf{C}}} P(h_0|x, I)\, dh_0\,, \tag{63}$$

which states that the true amplitude h_0 lies within $[0, h_0^{\mathbf{C}}]$ with a probability of $\mathbf{C}$. Note that this "confidence" $\mathbf{C}$ has an entirely different meaning than the frequentist confidence of Eq. (58).

3.5 Parameter space of coherent wide-parameter searches

As mentioned earlier, the sensitivity of wide-parameter (as opposed to targeted) searches is severely limited by the large number of required templates, which is rapidly increasing with the observation time T_{obs}. The measure of how densely templates need to be placed in the Doppler-parameter space is determined by the relative loss m in the detection statistic, $\mathcal{F}$ say, incurred by a Doppler-offset $d\boldsymbol{\lambda} = \boldsymbol{\lambda} - \boldsymbol{\lambda}_0$ from a putative signal position $\boldsymbol{\lambda}_0$. This mismatch m induces a natural distance measure and a corresponding local *metric* g_{ij} on the parameter space (first introduced by Balasubramanian et al. (1996) and Owen (1996)), namely

$$m(\boldsymbol{\lambda}_0, d\boldsymbol{\lambda}) = \frac{E[\mathcal{F}(\boldsymbol{\lambda}_0)] - E[\mathcal{F}(\boldsymbol{\lambda})]}{E[\mathcal{F}(\boldsymbol{\lambda}_0)]} = g_{ij}(\boldsymbol{\lambda}_0)\, d\boldsymbol{\lambda}^i\, d\boldsymbol{\lambda}^j + \mathcal{O}(d\boldsymbol{\lambda}^3)\,, \tag{64}$$

where we use the fact that $E[\mathcal{F}(\boldsymbol{\lambda}_0)]$ is a local maximum of $\mathcal{F}$ if there is a signal in $\boldsymbol{\lambda}_0$. It can be shown (cf. Brady et al., 1998) that the metric is approximately given by

$$g_{ij} \sim \langle \partial_i\phi\, \partial_j\phi\rangle - \langle \partial_i\phi\rangle\langle \partial_j\phi\rangle\,, \tag{65}$$

in terms of the signal phase $\phi(t)$, and where we defined $\partial_i = \partial/\partial\boldsymbol{\lambda}^i$ and $\langle . \rangle$ denotes the time-average over T_{obs}. Consider now the explicit phase model

(21), (24) for isolated neutron stars with one spindown, i.e. $\boldsymbol{\lambda}^i \in \{\boldsymbol{n}, f, \dot{f}\}$, for which one can easily show (e.g. Prix (2006)) the following scaling relations (of the dominant contributions), namely

$$g_{\theta\theta} \propto (f T_{\mathrm{obs}} V/c)^2 \,, \quad g_{ff} \propto T_{\mathrm{obs}}^2 \,, \quad g_{\dot{f}\dot{f}} \propto T_{\mathrm{obs}}^4 \,, \tag{66}$$

where θ is the angular separation on the sky and $V/c \sim 10^{-4}$ is the maximal Doppler shift due to the orbital velocity V. The required number of templates dN_p per small parameter-space region $d^4\boldsymbol{\lambda} = d\Omega \times df \times d\dot{f}$ (with sky solid-angle $d\Omega$) is therefore

$$dN_p \propto \sqrt{|\det g_{ij}|}\; d^4\boldsymbol{\lambda} \propto T_{\mathrm{obs}}^5\, f^2\, d^4\boldsymbol{\lambda} \,. \tag{67}$$

As noted in Prix (2006), the $\mathcal{O}(T_{\mathrm{obs}}^2)$ growth of the number of sky templates should only be considered as a lower bound, and a more detailed analysis is required to determine the exact scaling with T. Each template requires integrating (43), so the computing cost per template scales as $c_p \propto T_{\mathrm{obs}}$, and the total computing cost dC_p per parameter space $d^4\boldsymbol{\lambda}$ scales (at least) as

$$dC_p \propto T_{\mathrm{obs}}^6\, f^2\, d^4\boldsymbol{\lambda} \,. \tag{68}$$

This rapid growth of the computing cost $C_p(T_{\mathrm{obs}})$ severely limits the longest integration time T_{obs} that is affordable for all-sky, wide-frequency searches, to about $T_{\mathrm{obs}} \sim 10\,\mathrm{h} - 30\,\mathrm{h}$ with currently realistic levels of computing power, say ~ 50 Tflops with Einstein@Home (cf. Sec. 3.7). The second effect of the large number of templates N_p is to reduce the sensitivity compared to a targeted search with the *same* observation time and false-alarm probability: increasing the number of templates increases the number of expected false-alarm candidates at fixed detection threshold. Therefore the detection-threshold needs to be raised to maintain the same false-alarm rate, thereby decreasing the sensitivity.

Note that increasing the number of equal-sensitivity detectors $\mathcal{N}$ improves the SNR (45) in the same way as increasing the integration time T_{obs}. However, as shown recently (Prix, 2006), the metric expression (65) and the scaling (66) are still approximately valid even for such a network of detectors. This implies that increasing the number of detectors $\mathcal{N}$ does — contrary to the observation time T_{obs} — *not* increase the required number of templates N_p, which makes this the computationally cheapest way to improve the SNR of coherent wide-parameter searches.

3.6 Semi-coherent methods

Coherent matched-filtering is the optimal method for targeted, single-template searches. However, as suggested by the discussion in the previous section, wide-parameter searches will require techniques that trade off statistical "optimality" for higher speed (i.e. a smaller number of templates). These so-called

"semi-coherent" methods are less sensitive than matched filtering for the same observation time. However, as they require far fewer templates in parameter space, they can thereby over-compensate the loss of sensitivity by using a *longer* observation time and *lower* thresholds, which typically results in more sensitive searches at substantially smaller computing cost.

Here we focus on the simplest types of semi-coherent methods, which operate on successive short Fourier transforms (SFTs) of the measured strain $x(t)$. There are three main variants of such SFT-based semi-coherent methods currently in use for GW searches, known respectively as "StackSlide"[3], the "Hough transform" and "PowerFlux" (see Abbott et al. (2006a) for a more detailed description). All of these methods aim at detecting a statistical excess in the cumulative power of successive SFTs, following the correct time-frequency "path" of the signal frequency $f(t)$ at the detector, as illustrated in Fig. 1. The instantaneous frequency $f(t)$ of a signal at the detector can, to

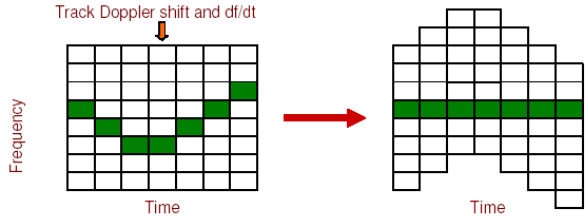

Fig. 1. An illustration of the principle used in semi-coherent methods to detect continuous GWs: The dark pixels represent a signal in the data. Its frequency changes with time (shown horizontally) due to Doppler shifts and intrinsic evolution of the source. By appropriately sliding the frequency bins of successive coherent "stacks" (shown vertically), the power of the signal can be lined up and summed.

a very good approximation (e.g. see Krishnan et al., 2004), be related to the instantaneous intrinsic frequency $f_{\mathrm{SSB}}(t)$ of isolated neutron stars by

$$f(t) = \left(1 + \frac{\mathbf{v}(t)\cdot\boldsymbol{n}}{c}\right) f_{\mathrm{SSB}}(t)\,, \tag{69}$$

where $\mathbf{v}(t)$ is the detector velocity with respect to the SSB frame. The total observation time T_{obs} is divided into N shorter "stacks" of duration $T_{\mathrm{coh}} = T_{\mathrm{obs}}/N$. The timeseries $x_j^{(l)}$ of stack l is then Fourier-transformed (42) with frequency bins $f_k = k/T_{\mathrm{coh}}$, which gives the SFT $\widetilde{x}_k^{(l)}$ for the stack l. The normalized power $\rho_k^{(l)}$ in the frequency-bin k of stack l is defined as

$$\rho_k^{(l)} \equiv \frac{2|\widetilde{x}_k^{(l)}|^2}{T_{\mathrm{coh}}\, S_{\mathrm{n}}}\,, \tag{70}$$

[3] Sometimes also referred to as the "Radon transform"

such that in the absence of a signal, the expectation value is $E[\rho_k^{(l)}] = 1$. The maximal length of SFT stacks is constrained (contrary to demodulated stacks, cf. Krishnan et al. (2004)) by the requirement that the signal power should not be spread over more than one frequency bin by the Doppler shift, which typically limits SFT stacks to about $T_{\mathrm{coh}} \lesssim 60$ min.

The *StackSlide* method computes the total power $P = N^{-1} \sum_l \rho_{k(l)}^{(l)}$ along the time-frequency path of bins $k(l)$ given by (69), as illustrated in Fig. 1. The *PowerFlux* method is a variant of StackSlide, summing *weighted* power in order to improve the sensitivity by taking account of non-stationarities of the noise and the direction-dependent antenna-patterns. The *Hough transform*, on the other hand, sums binary *number counts* $n_k^{(l)}$ instead of power. These number counts are obtained by setting a threshold ρ_{th} on the normalized power (70), namely $n_k^{(l)} = 1$ if $\rho_k^{(l)} \geq \rho_{\mathrm{th}}$, and $n_k^{(l)} = 0$ otherwise. The final Hough detection statistic is the total number count $n = \sum_l w_l n_{k(l)}^{(l)}$ of threshold-crossings along the time-frequency path $k(l)$, allowing for additional weights w_l that be tuned to improve the sensitivity. Summing binary number counts instead of power slightly reduces the sensitivity of the Hough method compared to StackSlide and PowerFlux, but it increases its robustness with respect to transient disturbances, as no single stack can contribute more than '1' to the final number count.

Semi-coherent methods combine a measure of power from different stacks, while the phase information between stacks is lost, which reduces the sensitivity compared to fully coherent matched filtering with the same observation time T_{obs}. This effect can be seen, for example, in the average amplitude h_0 of the weakest signal detectable in a targeted Hough-search with a 1% false-alarm rate and a 10% false-dismissal rate (Krishnan et al., 2004), namely

$$\langle h_0 \rangle_{\alpha=1\%}^{\beta=10\%} \approx 8.54\, N^{1/4} \sqrt{\frac{S_{\mathrm{n}}}{T_{\mathrm{obs}}}} = 8.54\, N^{-1/4} \sqrt{\frac{S_{\mathrm{n}}}{T_{\mathrm{coh}}}}\,, \tag{71}$$

where $N = T_{\mathrm{obs}}/T_{\mathrm{coh}}$ is the number of stacks. Similar expressions hold for StackSlide and PowerFlux, see Abbott et al. (2006a). Comparing this to the analogous matched-filtering expression (57) shows that a coherent search over the full observation time T_{obs} would be more sensitive by about a factor of $N^{1/4}$. On the other hand, combining N coherent searches using integration time T_{coh} would improve the sensitivity by about a factor of $N^{1/4}$. This relative loss in sensitivity, however, buys an enormous advantage, namely a substantially lower parameter-space resolution compared to a coherent search with the same T_{obs}. We can estimate the frequency resolution of the semi-coherent search as $\delta f \sim 1/T_{\mathrm{coh}}$, which is the natural frequency-resolution of the SFT stacks. The resolution in spindown $\delta \dot{f}$ and angular sky-position $\delta\theta$ can be estimated from the condition that the frequency should not drift by more than one frequency-bin δf over the total observation time T_{obs} (cf. Abbott et al., 2006a), which results in

$$\delta\dot{f} \sim \frac{1}{T_{\mathrm{obs}}\, T_{\mathrm{coh}}}\,, \quad \delta\theta \sim \frac{1}{f\, T_{\mathrm{coh}}\, V/c}\,. \tag{72}$$

The number of required templates per parameter-space $d^4\boldsymbol{\lambda}$ in a search for isolated neutron stars with one spindown therefore scales as

$$dN_p \propto T_{\mathrm{obs}}\, T_{\mathrm{coh}}^4\, f^2\, d^4\boldsymbol{\lambda}\,. \tag{73}$$

Each parameter-space point requires summing $N \propto T_{\mathrm{obs}}$ numbers, so the computing cost dC_p scales as

$$dC_p \propto T_{\mathrm{obs}}^2\, T_{\mathrm{coh}}^4\, f^2\, d^4\boldsymbol{\lambda}\,, \tag{74}$$

which shows that the increase in computing cost with T_{obs} is substantially slower than in the fully coherent case (68). This allows extending the search over much longer total observation times T_{obs}, of the order of several months instead of hours, and thereby achieving better sensitivity at lower computing cost than fully coherent matched-filtering. The semi-coherent methods are not restricted to using SFT stacks, one can also use demodulated stacks, such as the $\mathcal{F}$-statistic (53), as discussed in Krishnan et al. (2004). This allows to increase the length of the coherent stacks T_{coh} beyond the restriction $T_{\mathrm{coh}} \lesssim 1\mathrm{h}$ of SFT stacks, which improves the sensitivity (71), but also the computing cost (74).

3.7 Hierarchical searches and Einstein@Home

Neither the matched-filtering nor the semi-coherent methods described in the previous sections optimize by themselves the sensitivity of wide-parameter searches at given finite computing power: the sensitivity can be further improved by appropriately combining several stages of such coherent and semi-coherent steps, in what is generally known as "hierarchical" schemes (Brady and Creighton, 2000; Frasca et al., 2005; Cutler et al., 2005).

The general idea is to start with a wide-parameter search using a relatively short observation time and therefore low resolution in parameter space. In this first stage a low threshold is used in order to increase the chances of a weak signal crossing the threshold. This will result in a large number of random-chance candidates, however, which are followed up in a second stage search using a longer observation time and a higher threshold. This is computationally affordable due to the reduced number of templates required to follow up on the first-stage candidates, as opposed to scanning the entire parameter space at high resolution. The last step can be iterated several times with increasingly longer observation times and higher thresholds, successively gaining confidence in the surviving candidates. There are several free parameters in such a scheme, such as the number of stages, the length of respective stacks and their corresponding thresholds, all of which need to be optimized in order to obtain the best possible sensitivity per computing cost. A first

study of this optimization problem was carried out by Cutler et al. (2005), and the results suggest that about three stages might be sufficient.

In addition to the (still ongoing) effort to develop such an optimal search algorithm, one also wants to maximize the available computing power in order to optimize the absolute sensitivity of the search. This second goal is accomplished by the Einstein@Home project,[4] a public distributed-computing project launched in Feb. 2005. Einstein@Home is based on the distributed-computing platform BOINC,[5] which was originally developed for Seti@Home, and which is now used by a growing number of distributed-computing projects. The search for continuous GWs is ideally suited for this kind of distributed approach, as it can be split into a large number of small, independent problems: each participating host analyzes only a small portion $\Delta\boldsymbol{\lambda}$ of the total Doppler parameter space. After completing this search, the host returns the results to a central project server and requests the next "work-unit" to analyze. By Aug. 2006, Einstein@Home has attracted more than 100,000 participants, contributing more than 200,000 CPUs, and delivering more than 50 Tflops of continuous computing power. The hierarchical search scheme currently under development for Einstein@Home is ultimately expected to yield the most sensitive wide-parameter search available for continuous GWs from unknown spinning neutron stars.

4 Current status of the search for continuous GWs

4.1 The Detectors

Starting from the pioneering efforts of Joseph Weber in the early 1960's, the first GW detectors were based on the principle of monitoring the oscillations of massive resonant metal bars, the so-called bar detectors. A GW at or near the resonance frequency of the bar would excite this oscillation mode. These designs have been successively improved over time, and today there are still a number of bar detectors operating, including ALLEGRO in Louisiana, EXPLORER at CERN and NAUTILUS in Rome. During the past decade, however, several scientific collaborations have constructed large-scale interferometric GW detectors. These include the Laser Interferometer Gravitational Wave Observatory (LIGO), consisting of three interferometers, built by a Caltech-MIT collaboration (Abramovici et al., 1992); the GEO 600 detector built by a British-German collaboration (Willke et al., 2002); the Virgo detector built by an Italian-French collaboration (Caron et al., 1997); and the Japanese TAMA 300 detector in Tokyo (Tsubono, 1995). In all of these detectors, the relative displacement of suspended test masses is sensed interferometrically, as illustrated in Fig. 2. As discussed in Sec. 1, a GW produces

[4] `http://einstein.phys.uwm.edu/`
[5] `http://boinc.berkeley.edu/`

a time-varying differential displacement δl of the test masses that is proportional to the arm length l of the interferometer, so the measured dimensionless strain is $h(t) = \delta l/l$.

In the following we will mainly focus on the detectors run within the LIGO Scientific Collaboration (LSC), namely LIGO and GEO 600. LIGO consists of three interferometers installed at two sites: the Livingston site (Louisiana) contains one interferometer of 4 km armlength (referred to as L1), while the Hanford site (in Washington state) houses two interferometers, one of 4 km and one of 2 km armlength (called H1 and H2, respectively). In all four instru-

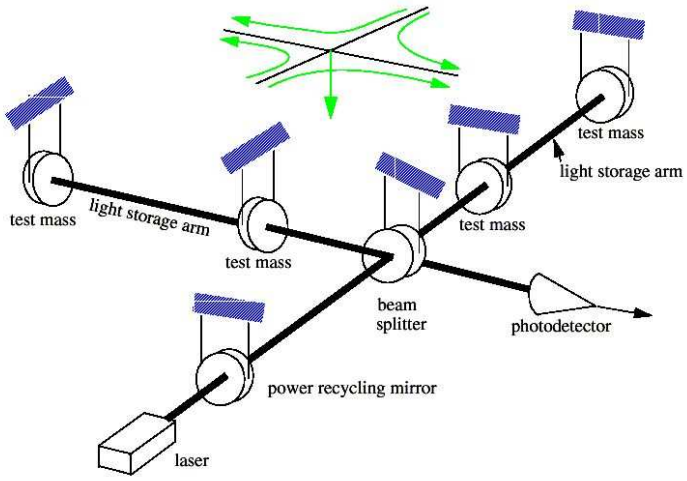

Fig. 2. Schematic layout of an interferometric gravitational-wave detector with power recycling. The quadrupolar strain deformation-field above the detector indicates an incident GW with optimal orientation.

ments (H1, H2, L1, G1), the beam splitters, recycling mirrors and test masses are hung as pendulums from multilayer seismic isolation filters to isolate them from local forces (see Fig. 2). The masses and beam paths are housed in high vacuum enclosures to avoid optical scintillation and acoustic interference.

4.2 LIGO/GEO600 Sensitivities and Scientific Runs

LIGO and (partially) GEO600 have so far completed four science-mode data-taking runs (denoted S1-S4), and a fifth science run (S5) is currently underway (see Table 1 for a summary). The "duty cycle" in Table 1 refers to the percentage of the run time where the detector was "in lock" and was taking science data. Due to ground motion, equipment failures and alignment drifts, the duty cycle is generally less than 100%. Livingston (L1) had particularly low

Run	Start – End	best sensitivity $\sqrt{S_n}\,[\mathrm{Hz}^{-1/2}]$	duty cycles [%] H1	L1	H2	G1
S1	Aug 23 – Sept 9, 2002	2×10^{-21}	57.6	41.7	73.1	98.5
S2	Feb 14 – Apr 14, 2003	2×10^{-22}	73.5	36.9	57.8	–
S3	Oct 31, 2003 – Jan 9, 2004	5×10^{-23}	69.3	21.8	63.4	96.9†
S4	Feb 22 - Mar 23, 2005	4×10^{-23}	80.5	74.5	81.4	96.6
S5*	Nov 4, 2005 - ∼Aug, 2007	2×10^{-23}	71.0	59.1‡	78.2	80.4

Table 1. Summary of LIGO/GEO600 scientific runs. †Partial participation: Nov 5, 03 – Nov 12, 03 and Dec 30, 03 – Jan 13, 04, ‡started Nov 14, 05, * status in Aug, 06

duty-cycles during S1 to S3 due to anthropogenic low-frequency noise (logging activity in a nearby forest). This problem has been largely overcome by installing an improved (active) seismic isolation before the start of S4, which resulted in dramatic improvements in the L1 duty cycle, as seen in Table 1. GEO 600 has currently the best duty cycles, but also lower sensitivity than LIGO, cf. Fig. 3. As seen in this figure, the LIGO detectors have reached their

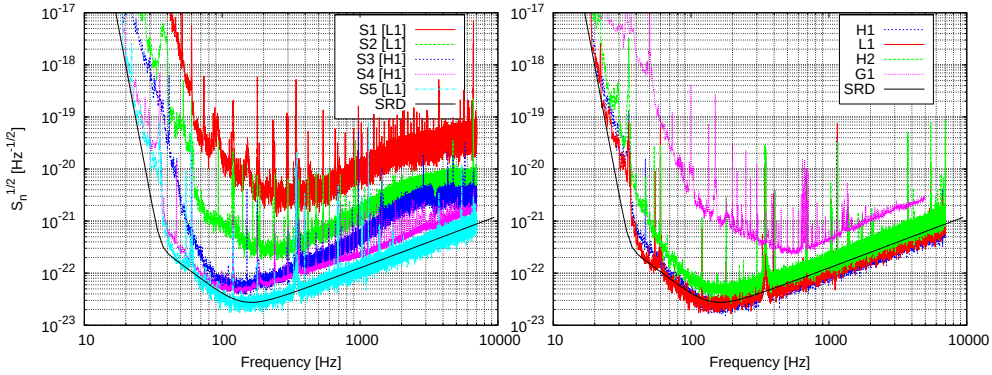

Fig. 3. *Left figure:* Successive best LIGO sensitivities over the 5 science runs S1 - S5. *Right figure:* LIGO and GEO600 sensitivities during S5 (as of June 2006).

design sensitivity with the S5 run, which will be taking one year of coincident data (the run will last for about 2 years). After S5, Initial LIGO will undergo some enhancements, followed by another long science run (S6). After S6, work will start on the next-generation Advanced LIGO detector, which will be installed on the same sites as Initial LIGO, and which is planned to start taking data within a decade.

4.3 Overview of continuous-wave searches

A summary plot of the current status of the search for continuous GWs from spinning neutron stars is given in Fig. 4. This figure shows *approximate* lev-

els of published upper limits, *estimated* sensitivities of current and future searches, and astrophysically motivated upper limits. The spindown upper

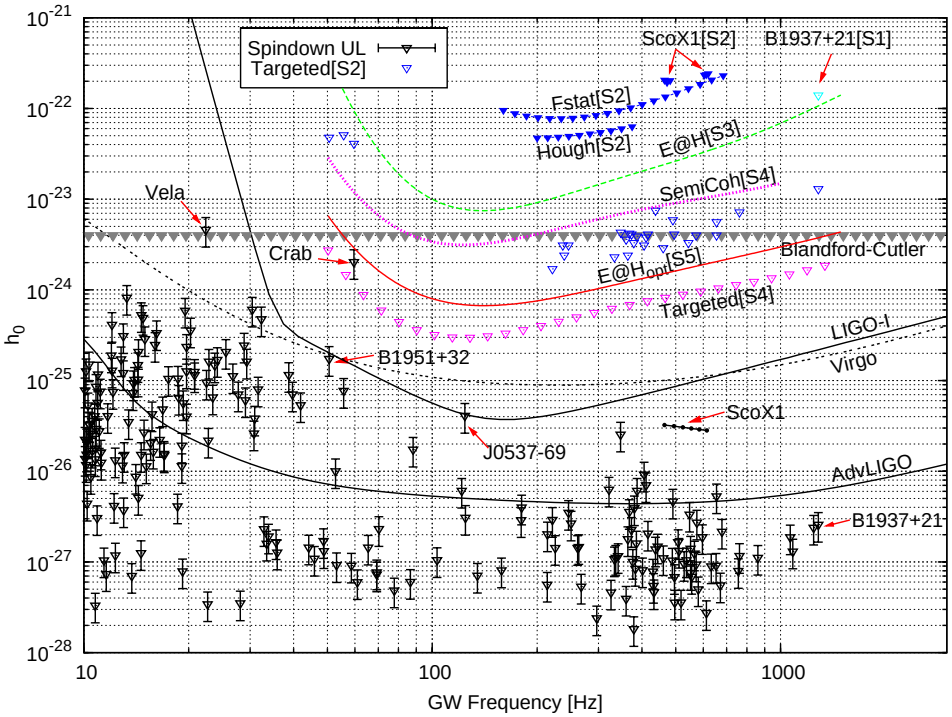

Fig. 4. Summary plot of the approximate levels of published upper limits (cf. Sec. 4.4), estimated sensitivities of some current and future searches (cf. Sec. 4.5) and astrophysical upper limits (cf. Sec. 4.3). The 'Blandford-Cutler' limit refers to the statistical argument for isolated neutron stars mentioned in Sec. 2.2, Eq. (13).

limits (17) for known pulsars in Fig. 4 are based on the pulsar parameters from known pulsars in the ATNF catalog (Manchester et al., 2005), allowing for a distance uncertainty of $\pm 10\%$ and a moment of inertia in the range $I_{zz} = (1-3)\times 10^{38}\,\mathrm{kg\,m^2}$ (see Abbott et al. (2006c) for discussion). The astrophysical limit for Sco X-1 is based on the Bildsten-Wagoner mechanism (19). The *design* curves 'LIGO-I', 'Virgo' and 'AdvLIGO' in Fig. 4, are described by Eq. (57), and assume a targeted coherent integration of one year of data at the respective design sensitivity, whereby LIGO-I and Advanced LIGO consist of networks of three detectors (H1+H2+L1). Note that these sensitivities can only be reached in targeted searches for known pulsars, assuming ideal conditions of well-constrained parameters (e.g. negligible timing-noise and no glitches). As discussed in Sec. 3.5, wide-parameter searches are inherently less sensitive due to the large number of templates required.

4.4 Results from completed searches

S1: targeted search for PSR B1937+21

The fully coherent methods described in Sec. 3.3 and Sec. 3.4 were used to perform a targeted search for the millisecond pulsar PSR B1937+21, using data from the first LIGO science run (S1) (Abbott et al., 2004b). The Doppler parameters (sky-position + spin) of this pulsar are well known and are extremely stable, which allows a single-template search. From the spindown upper limit for this pulsar (cf. Fig. 4), it is obvious that no detection was expected, the motivation for this search was mainly to illustrate the methods and set an upper limit on the GW emission at $f = 2\nu$. The resulting best upper limit obtained was $h_0^{95\%} \sim 1.4 \times 10^{-22}$.

S2: $\mathcal{F}$-statistic wide-parameter search for Sco X-1

A coherent wide-parameter $\mathcal{F}$-statistic search for Sco X-1 was performed (Abbott et al., 2006b) using data from the S2 science run. Sco X-1 is a neutron star in a 18.9 h orbit around a low-mass companion, at a distance of $d \sim 2.8$ kpc from Earth. The sky-position $\boldsymbol{n}$ and orbital period P of Sco X-1 are well determined from X-ray observations, but both the projected semi-major axis a_p and the orbital phase $\bar{T}$ have large uncertainties and need to be treated as unknown (Doppler) parameters. The rotation frequency ν of the neutron star is also highly uncertain. Assuming the (not uncontroversial) beat-frequency model for QPOs (van der Klis et al., 1997), and a triaxial neutron star emitting GWs at a frequency $f = 2\nu$, the frequency window of the search would span at least $f \in [460, 620]$ Hz. Due to the enormous computational cost of this search, however, this had to be reduced to two interesting bands $f \in [464, 484]$ Hz and $f \in [604, 624]$ Hz. The scaling of the number of templates N_p for this Doppler parameter space ($\boldsymbol{\lambda} = \{f, a_p, \bar{T}\}$) is $N_p \propto T_{\mathrm{obs}}^6$, which severely limited the maximum possible observation time T_{obs}. The analysis pipeline consisted of two $\mathcal{F}$-statistic searches over the most sensitive $T_{\mathrm{obs}} = 6$ h of data from L1 and H1 respectively, followed by a coincidence step to reduce the number of false-alarm candidates. Upper limits of the order $h_0^{95\%} \sim 2 \times 10^{-22}$ were obtained over the range of parameters analyzed (labeled 'ScoX1[S2]' in Fig. 4).

S2: $\mathcal{F}$-statistic all-sky search for unknown isolated neutron stars

A similar wide-parameter search with the $\mathcal{F}$-statistic was performed for unknown isolated neutron stars over the whole sky and in the frequency range $f \in [160, 729]$ Hz, assuming a frequency-derivative of less than $|\dot{f}| < 4 \times 10^{-10}$ Hz/s. The scaling of the number of templates with observation time T_{obs} for this Doppler space $\boldsymbol{\lambda} = \{\alpha, \delta, f\}$ is $N_p \propto T_{\mathrm{obs}}^3$, see Sec. 3.5. The analysis followed a similar pipeline to the Sco X-1 search, using the most sensitive $T_{\mathrm{obs}} = 10$ h of data from L1 and H1, respectively, and reducing the false-alarm rate by a coincidence step. The best all-sky (frequentist) upper limit achieved was of the order $h_0^{95\%} \sim 7 \times 10^{-23}$, as shown in Fig. 4 (label 'Fstat[S2]').

S2: Hough all-sky search for unknown isolated neutron stars

The Hough-transform method (cf. Sec. 3.6) was used in an all-sky search for unknown isolated neutron stars (Abbott et al., 2005a) in the frequency range $f \in [200, 400]$ Hz, including one spindown parameter $\dot{f} \in [-10^{-9}, +10^{-10}]$ Hz/s. The data from all three LIGO detectors was analyzed over the *whole* duration of $T_{\rm obs} = 2$ months of S2. This required searching of the order $N_p \sim 10^{12}$ templates (many orders of magnitude less than a coherent search would require for the same $T_{\rm obs}$), which took less than half a day to complete on a 200-CPU cluster. The best all-sky upper limit obtained in this frequency-range was $h_0^{95\%} \sim 4.4 \times 10^{-23}$, and the results are summarized in Fig. 4 (label 'Hough[S2]'). The sensitivity achieved by this semi-coherent search is about a factor of *two* better than the equivalent $\mathcal{F}$-statistic search ('Fstat[S2]'), which required similar computing power. This is a consequence of the lower parameter-space resolution of semi-coherent methods, therefore allowing to use the full two months of data as opposed to only 10 hours (cf. Sec. 3.6).

S2: targeted search for 28 known pulsars

The results from a targeted, fully coherent search for 28 known isolated radio pulsars in the LIGO band ($f = 2\nu \gtrsim 50$ Hz) have been reported in Abbott et al. (2005b). The analysis was based on the Bayesian approach described in Sec. 3.4, and the actual implementation used a highly efficient complex-heterodyning method described in Dupuis and Woan (2005). Data from the S2 science run was analyzed, combining H1, L1 and H2 coherently (GEO600 did not take part in S2). The resulting Bayesian 95% confidence upper limits are shown in Fig. 4 (label 'Targeted[S2]'). Most of these upper limits are still a few orders of magnitude above the corresponding spindown limits (when available), but for the globular-cluster pulsars with apparent spin-up, these are the first direct constraints available. The best strain upper limit obtained was $h_0^{95\%} \sim 1.7 \times 10^{-24}$ (for PSR J1910-5959D), and the best upper limit on the quadrupolar deformation was $\epsilon^{95\%} \sim 4.5 \times 10^{-6}$ (for PSR J2124-3358). The upper limit for the Crab pulsar (PSR B0531+21) was $h_0^{95\%} \sim 4 \times 10^{-23}$, which is within a factor of 30 from the spindown upper limit. As discussed in Sec. 3.5, fully coherent targeted searches provide the best possible sensitivity, which is illustrated by these results: at similar computing cost, the targeted S2 search is about 25 times more sensitive than the semi-coherent searches, and about 50 times more sensitive than the fully coherent wide-parameter searches.

4.5 Ongoing and future searches

Einstein@Home: S3 and beyond

Einstein@Home (cf. Sec. 3.7) has completed a search on $T_{\rm obs} = 600$ h of LIGO S3 data, and the results have been posted online (Abbott et al., 2005c).

The analysis pipeline consisted of $N = 60$ stacks (of $T_{\mathrm{coh}} = 10$ h each) of coherent all-sky, wide-frequency searches using the $\mathcal{F}$-statistic. This coherent step was performed on the participating hosts and the results were returned to the central server for post-processing, where they were combined using a stacking/coincidence scheme.

Einstein@Home is aiming for a detection, and no upper limits have been set so far. In order to obtain a rough estimate of the *approximate* level of sensitivity, we will assume (somewhat optimistically) that the post-processing step results in a $\propto N^{1/4}$ improvement in sensitivity, as would be typical for semi-coherent methods (71). However, the pre-factor in (71) depends on the threshold $2\mathcal{F}^*$ used in the coherent stacks of $\mathcal{F}$-statistic integrations. For Einstein@Home we had to choose a relatively high threshold of $2\mathcal{F}^* = 25$, in order to limit the total amount of (false-alarm) data sent back to the central server for post-processing. We therefore use Eq. [6.40] of Krishnan et al. (2004) to estimate the correct pre-factor in (71), and (adding an extra factor of 2 to account for the average mismatch) we find ~ 66 instead of 8.54. The corresponding sensitivity-estimate is plotted in Fig. 4 (label 'E@H[S3]'). A similar search was performed on S4 data, using a total of $T_{\mathrm{obs}} = 510$ h of data divided in $N = 17$ stacks of $\mathcal{F}$-statistic integrations over $T_{\mathrm{coh}} = 30$ h. The results from this run are currently in the post-processing stage. A search on S5 data using the same pipeline is currently ongoing, using $N = 28$ stacks of $T_{\mathrm{coh}} = 30$ h.

The sensitivity of these searches suffers from the same problem as the S3 search due to the required high $2\mathcal{F}^*$ threshold. This limitation, however, should be overcome in the setup for the next Einstein@Home search, which will include a semi-coherent Hough step *on* the host, possibly followed by another, longer $\mathcal{F}$-statistic integration, as described in Sec. 3.7. This hierarchical approach will substantially reduce the amount of (false-alarm) data that needs to be sent back, allowing for a much lower $2\mathcal{F}^*$ threshold. Ideally it should be possible to use the optimal threshold of $2\mathcal{F}^* = 5.2$ (Krishnan et al., 2004). We can therefore estimate the "optimal" sensitivity of such an Einstein@Home search, assuming the current S5 setup of $T_{\mathrm{obs}} = 840$ h and $T_{\mathrm{coh}} = 30$ h, but using the optimal $2\mathcal{F}^*$ threshold. This yields a pre-factor of ~ 18 in Eq. (71), and the corresponding extrapolated sensitivity estimate is shown in Fig. 4, labeled '$\mathrm{E@H_{opt}}$[S5]'.

S4: Semi-coherent searches

An all-sky search for unknown isolated neutron stars in the frequency range $f \in [50, 1000]$ Hz on data from the S4 run ($T_{\mathrm{obs}} \sim 500$ h) was completed using the semi-coherent methods described in Sec. 3.6, namely Hough, StackSlide and PowerFlux. The stacks consisted of SFTs of duration $T_{\mathrm{coh}} = 30$ min, and data from all three LIGO interferometers was used. A paper presenting these results is currently in preparation. The expected sensitivity for these

searches can be directly estimated from Eq. (71), and is shown in Fig. 4 (label 'SemiCoherent[S4]').

S4, S5: Coherent targeted searches for known pulsars

Using the S4 data from all three LIGO interferometers and GEO600, a fully coherent targeted search for known pulsars (at $f = 2\nu$) was recently completed, and a paper presenting the results is currently in preparation. We can estimate the expected average sensitivity of this search by Eq. (57), and this estimate is shown in Fig. 4 (label 'Targeted[S4]'). This search would already seem to beat the spindown limit of the Crab pulsar, but unfortunately this is not the case: the noise is less stationary at lower frequencies and there are also some side-effects from the strong disturbance at 60 Hz from the mains power-line frequency in the US (visible in Fig. 3). As a result the Crab pulsar will still be a factor of a few above the spindown limit with the S4 search. Using several months of S5 data, however, it is expected that the Crab spindown limit will be beaten for the first time. This will be the *first* astrophysically relevant upper limit set on the GW emission of any pulsar.

4.6 Previous upper limits from other detectors

Bar detectors: an earlier attempt to specifically target the Crab pulsar (at $f = 2\nu \sim 60$ Hz) was made with a specially-designed bar detector (Suzuki, 1995), setting an upper limit of $h_0 \leq 2 \times 10^{-22}$. A search targeting the millisecond pulsar PSR B1937+21 (at $f = 2\nu \sim 1284$ Hz) was performed by Hough et al. (1983) using a split bar detector, producing an upper limit of $h_0 < 10^{-20}$. A search for unknown isolated neutron stars in a small frequency-band $f = (921.35 \pm 0.03)$ Hz and a small sky-region in the galactic center was performed using 95 days of data from the EXPLORER bar detector, and an upper limit of $h_0 \sim 3 \times 10^{-24}$ was obtained (Astone et al. (2002)). An all-sky search with two days of EXPLORER data in the frequency-band $f = (921.38 \pm 0.38)$ Hz was carried out using the $\mathcal{F}$-statistic, setting an upper limit of $h_0^{99\%} \sim 2 \times 10^{-23}$, reported in Astone et al. (2003). This, was later revised to $h_0^{90\%} \sim 10^{-22}$ in Astone et al. (2005) using different conventions to determine the upper-limit. Another directed search was presented in Mauceli et al. (2000): data from the ALLEGRO bar detector was searched for periodic GWs from the Galactic center and from the globular cluster 47 Tuc in the two antenna bands (896.80 ± 0.50) Hz and (920.26 ± 0.50) Hz, setting an upper limit of $h_0 \sim 8 \times 10^{-24}$.

Interferometers: the first search using a broadband interferometer was carried out with the prototype 40 m detector at Caltech by Hereld (1984). The search was targeting PSR B1937+21, and resulted in upper limits of the order $h_0 \lesssim 3 \times 10^{-17}$ at $f = \nu$, and $h_0 \lesssim 1.5 \times 10^{-17}$ at $f = 2\nu$. Data from the first science run of the TAMA detector was searched for continuous GWs from SN1987A using coherent matched filtering over $T_{\rm obs} = 1200$ h of data in a

0.05 Hz band at ~ 934.9 Hz, and the reported upper limit (Soida et al., 2003) was about $h_0^{99\%} \sim 5 \times 10^{-23}$. An earlier upper-limit result on SN1987A was obtained from a directed search using $T_{\mathrm{obs}} = 100$ h of data from the Garching prototype interferometer, which determined an upper limit of $h_0^{95\%} \sim 9{\times}10^{-21}$ in 4 Hz bands around $f = \nu \sim 1670$ Hz and $f = 2\nu$ (Niebauer et al., 1993).

5 Outlook

LIGO has made enormous progress over the past 4 years, as seen Fig. 3, reaching its design sensitivity with the S5 science run. This progress in sensitivity is also reflected in the improving sensitivities of the continuous-wave searches shown in Fig. 4. While a detection of a spinning neutron star with LIGO-I is somewhat unlikely (albeit not implausible), the LIGO continuous-wave searches are beginning to enter a regime of increasing astrophysical relevance: **(i)** A targeted pulsar search with S5 will almost certainly beat the spindown upper limit for the Crab pulsar. This will be the first time that GW observations set an astrophysical constraint on the contribution to the observed pulsar spindown. **(ii)** With one year of data from S5 (and possibly S6 with enhanced LIGO), the spindown limits of two more pulsars (J0537-6910 and B1951+32) can be (marginally) reached. **(iii)** The upper limits on the non-axisymmetry ϵ of known pulsars are beginning to enter the regime $\epsilon \lesssim 10^{-6}$, which is considered physically possible according to our current understanding of neutron-star physics (cf. Sec. 2.1). **(iv)** The statistical upper-limit level $h_0 \lesssim 4 \times 10^{-24}$ set by the Blandford-Cutler argument on unknown isolated neutron stars (cf. Sec. 2.2) has been marginally reached by the semi-coherent searches using S4 data, and will be substantially surpassed by semi-coherent and Einstein@Home/hierarchical searches using S5, and even more so using S6. Passing this milestone suggests that the possibility of a detection of an unknown isolated neutron star is becoming increasingly plausible.

Furthermore, the Virgo detector will start observing within the next year or two. Once it has reached its design sensitivity, Virgo should be able to beat the spindown limit of up to three more known pulsars (including Vela), as seen in Fig. 4. Combining Virgo with the LIGO detector network will result in a further increase of $\sim 20\%$ in average sensitivity with respect to LIGO-I.

However, Advanced LIGO will be by far the most exciting instrument in the near future for GW searches from neutron stars, as can see in Fig. 4. It will allow to surpass the spindown limits of several tens of known pulsars with one year of data, and it will comfortably cover the Bildsten-Wagoner emission-level (19) of Sco X-1 (assuming, however, that substantially better observational constraints on the Sco X-1 parameters are available for a directed search). Advanced LIGO will dig down up to three orders of magnitude below the Blandford-Cutler threshold, making a detection of neutron-star signals seem rather likely.

Given the current progress and the encouraging prospects about the future developments, it seems reasonable to be optimistic that gravitational-wave astrophysics of neutron stars could finally become a reality within the next one or two decades.

Acknowledgement. The authors gratefully acknowledge the support of the United States National Science Foundation for the construction and operation of the LIGO Laboratory and the Particle Physics and Astronomy Research Council of the United Kingdom, the Max-Planck-Society and the State of Niedersachsen/Germany for support of the construction and operation of the GEO600 detector. The authors also gratefully acknowledge the support of the research by these agencies and by the Australian Research Council, the Natural Sciences and Engineering Research Council of Canada, the Council of Scientific and Industrial Research of India, the Department of Science and Technology of India, the Spanish Ministerio de Educacion y Ciencia, The National Aeronautics and Space Administration, the John Simon Guggenheim Foundation, the Alexander von Humboldt Foundation, the Leverhulme Trust, the David and Lucile Packard Foundation, the Research Corporation, and the Alfred P. Sloan Foundation. This document has been assigned LIGO Laboratory document number LIGO-P060039-00-Z.

References

Abbott, B. et al. (LIGO Scientific Collaboration): 2004a, *Nucl. Instrum. Methods Phys. Res. A* **517**, 154,

Abbott, B. et al. (LIGO Scientific Collaboration): 2004b, *Phys. Rev. D.* **69**, 082004,

Abbott, B. et al. (LIGO Scientific Collaboration): 2005a, *Phys. Rev. D.* **72**, 102004,

Abbott, B. et al. (LIGO Scientific Collaboration): 2005b, *Phys. Rev. Lett.* **94**, 181103,

Abbott, B. et al. (LIGO Scientific Collaboration): 2005c, *Report on Einstein@Home S3 analysis*, http://einstein.phys.uwm.edu/,

Abbott, B. et al. (LIGO Scientific Collaboration): 2006a, *in preparation*,

Abbott, B. et al. (LIGO Scientific Collaboration): 2006b, *submitted*, (preprint gr-qc/0605028)

Abbott, B. et al. (LIGO Scientific Collaboration): 2006c, *in preparation*,

Abramovici, A. et al.: 1992, *Science* **256**, 325

Abramowitz, M. and Stegun, I. A.: 1964, *Handbook of Mathematical Functions*, National Bureau of Standards

Andersson, N.: 1998, *ApJ* **502**, 708

Andersson, N.: 2003, *Class. Quant. Grav.* **20**, 105

Andersson, N., Jones, D. I., and Kokkotas, K. D.: 2002, *MNRAS* **337**, 1224

Andersson, N. and Kokkotas, K. D.: 1998, *MNRAS* **299**, 1059

Andersson, N., Kokkotas, K. D., and Stergioulas, N.: 1999, *ApJ* **516**, 307

Astone, P. et al.: 2002, *Phys. Rev. D.* **65(2)**, 022001

Astone, P. et al.: 2003, *Class. Quant. Grav.* **20**, 665
Astone, P. et al.: 2005, *Class. Quant. Grav.* **22**, 1243
Baiotti, L. et al.: 2006, (preprint astro-ph/0609473)
Balasubramanian, R., Sathyaprakash, B. S., and Dhurandhar, S. V.: 1996, *Phys. Rev. D.* **53**, 3033
Bildsten, L.: 1998, *ApJ* **501**, L89
Bonazzola, S. and Gourgoulhon, E.: 1996, *A&A* **312**, 675
Bonazzola, S. and Gourgoulhon, E.: 1997, in J.-A. Marck and J.-P. Lasota (eds.), *Relativistic Gravitation and Gravitational Radiation*, p. 151
Brady, P. R. and Creighton, T.: 2000, *Phys. Rev. D.* **61(8)**, 082001
Brady, P. R., Creighton, T., Cutler, C., and Schutz, B. F.: 1998, *Phys. Rev. D.* **57**, 2101
Caron, B., Dominjon, A., Drezen, C., Flaminio, R., et al.: 1997, *Nuclear Physics B Proceedings Supplements* **54**, 167
Carter, B., Langlois, D., and Sedrakian, D. M.: 2000, *A&A* **361**, 795
Centrella, J. M., New, K. C. B., Lowe, L. L., and Brown, J. D.: 2001, *ApJL* **550**, L193
Chakrabarty, D. et al.: 2003, *Nature* **424**, 42
Chandrasekhar, S.: 1970, *Phys. Rev. Lett.* **24**, 611
Christensen, N., Dupuis, R. J., Woan, G., and Meyer, R.: 2004, *Phys. Rev. D.* **70(2)**, 022001
Cook, G. B., Shapiro, S. L., and Teukolsky, S. A.: 1994, *ApJ* **424**, 823
Cutler, C.: 2002, *Phys. Rev. D.* **66**, 084025
Cutler, C., Gholami, I., and Krishnan, B.: 2005, *Phys. Rev. D.* **72(4)**, 042004
Cutler, C. and Jones, D. I.: 2001, *Phys. Rev. D.* **63(2)**, 024002
Cutler, C. and Schutz, B. F.: 2005, *Phys. Rev. D.* **72**, 063006
Dupuis, R. J. and Woan, G.: 2005, *Phys. Rev. D.* **72(10)**, 102002
Feldman, G. J. and Cousins, R. D.: 1998, *Phys. Rev. D.* **57**, 3873
Finn, L. S.: 1992, *Phys. Rev. D.* **46(12)**, 5236
Frasca, S., Astone, P., and Palomba, C.: 2005, *Class. Quant. Grav.* **22**, 1013
Friedman, J. L. and Morsink, S. M.: 1998, *ApJ* **502**, 714
Friedman, J. L. and Schutz, B. F.: 1978, *ApJ* **222**, 281
Hereld, M.: 1984, *Ph.D. Thesis (Caltech)*
Hough, J. et al.: 1983, *Nature* **303**, 216
Jaranowski, P. and Krolak, A.: 1994, *Phys. Rev. D.* **49**, 1723
Jaranowski, P. and Królak, A.: 2005, *Living Reviews in Relativity* **8**, 3, `http://relativity.livingreviews.org/Articles/lrr-2005-3`
Jaranowski, P., Królak, A., and Schutz, B. F.: 1998, *Phys. Rev. D.* **58**, 063001
Jones, D. I. and Andersson, N.: 2002, *MNRAS* **331**, 203
Kittel, C.: 2005, *Introduction to solid state physics*, Wiley, 8th edition
Krishnan, B. et al.: 2004, *Phys. Rev. D.* **70**, 802001
Loredo, J. T.: 1990, in P. F. Fougère (ed.), *Maximum Entropy and Bayesian Methods*, pp 81–142, Kluwer Academic Publishers, Netherlands
Manchester, R. N. et al.: 2005, *Astron. J.* **129**, 1993, `http://www.atnf.csiro.au/research/pulsar/psrcat/`

Mauceli, E. et al.: 2000, (preprint gr-qc/0007023)
Melatos, A. and Payne, D. J. B.: 2005, *ApJ* **623**, 1044
Misner, C. W., Thorne, K. S., and Wheeler, J. A.: 1973, *Gravitation*, W. H. Freeman and Company (New York)
Niebauer, T. M. et al.: 1993, *Phys. Rev. D.* **47**, 3106
Owen, B. J.: 1996, *Phys. Rev. D.* **53**, 6749
Owen, B. J.: 2005, *Phys. Rev. Lett.* **95**, 211101
Owen, B. J.: 2006, *Class. Quant. Grav.* **23**, 1
Owen, B. J. et al.: 1998, *Phys. Rev. D.* **58**, 084020
Papaloizou, J. and Pringle, J. E.: 1978, *MNRAS* **184**, 501
Payne, D. J. B. and Melatos, A.: 2006, *ApJ* **641**, 471
Prix, R.: 2006, *submitted*, (preprint gr-qc/0606088)
Ruderman, M.: 1969, *Nature* **223**, 597
Ruderman, M.: 1976, *ApJ* **203**, 213
Saijo, M. and Gourgoulhon, E.: 2006, (preprint astro-ph/0606569)
Schutz, B. F. and Tinto, M.: 1987, *MNRAS* **224**, 131
Shapiro, S. L. and Zane, S.: 1998, *ApJS* **117**, 531
Sivia, D. S.: 1996, *Data Analysis. A Bayesian Tutorial*, Oxford Science Publications
Soida, K. et al.: 2003, *Class. Quant. Grav.* **20**, 645, (TAMA Collaboration)
Stergioulas, N.: 2003, *Living Reviews in Relativity* **6**, 3, `http://relativity.livingreviews.org/Articles/lrr-2003-3/`
Suzuki, T.: 1995, in E. Coccia, G. Pizzella, and F. Ronga (eds.), *First Edoardo Amaldi Conference on Gravitational Wave Experiments*, p. 115
Taylor, J. H. and Weisberg, J. M.: 1989, *ApJ* **345**, 434
Thorne, K. S.: 1980, *Reviews of Modern Physics* **52**, 299
Thorne, K. S.: 1987, in S. W. Hawking and W. Israel (eds.), *300 Years of Gravitation*, Chapt. 9, p. 330, Cambridge University Press
Tsubono, K.: 1995, in E. Coccia, G. Pizzella, and F. Ronga (eds.), *First Edoardo Amaldi Conference on Gravitational Wave Experiments*, p. 112
Ushomirsky, G., Cutler, C., and Bildsten, L.: 2000, *MNRAS* **319**, 902
Van Den Broeck, C.: 2005, *Class. Quant. Grav.* **22**, 1825
van der Klis, M., Wijnands, R. A. D., Horne, K., and Chen, W.: 1997, *ApJL* **481**, L97
Wagoner, R. V.: 1984, *ApJ* **278**, 345
Wagoner, R. V.: 2002, *ApJ* **578**, L63
Wainstein, L. and Zubakov, V.: 1962, *Extraction of Signals from Noise*, Prentice-Hall, Englewood Cliffs
Watts, A. L. and Strohmayer, T. E.: 2006, (preprint astro-ph/0608476)
Weisberg, J. M. and Taylor, J. H.: 1984, *Phys. Rev. Lett.* **52**, 1348
Willke, B., Aufmuth, P., Aulbert, C., Babak, S., et al.: 2002, *Class. Quant. Grav.* **19**, 1377
Zimmermann, M. and Szedenits, Jr., E.: 1979, *Phys. Rev. D.* **20**, 351